AGU PUBLICATIONS

Geochemistry, Geophysics, Geosystems

RESEARCH ARTICLE
10.1002/2016GC006296

Sources and turnover of organic carbon and methane in fjord and shelf sediments off northern Norway

Simone Sauer[1,2], Wei-Li Hong[2], Jochen Knies[1,2], Aivo Lepland[1,2], Matthias Forwick[3], Martin Klug[1], Florian Eichinger[4], Soma Baranwal[2], Antoine Crémière[1,2], Shyam Chand[1,2], and Carsten J. Schubert[5]

[1]Geological Survey of Norway, Trondheim, Norway, [2]CAGE—Centre for Arctic Gas Hydrate, Environment and Climate, Department of Geology, UiT, The Arctic University of Norway, Tromsø, Norway, [3]Department of Geology, UiT, The Arctic University of Norway, Tromsø, Norway, [4]Hydroisotop GmbH, Schweitenkirchen, Germany, [5]Eawag, Swiss Federal Institute of Aquatic Science and Technology, Kastanienbaum, Switzerland

Key Points:
- Different processes control organic carbon and methane cycling in sediments on the shelf and in a fjord on the northern Norwegian margin
- Carbon for biogeochemical reactions in sediments supplied by marine organic matter in the fjord and by thermogenic CH_4 ascent on the shelf
- The fraction of depth-integrated sulfate reduction coupled to AOM is 97% on the shelf and 40% in the fjord

Supporting Information:
- Supporting Information S1
- Data Set S1

Correspondence to:
S. Sauer,
simone.sauer@ngu.no

Citation:
Sauer, S., et al. (2016), Sources and turnover of organic carbon and methane in fjord and shelf sediments off northern Norway, *Geochem. Geophys. Geosyst.*, *17*, 4011–4031, doi:10.1002/2016GC006296.

Received 4 FEB 2016
Accepted 29 SEP 2016
Accepted article online 4 OCT 2016
Published online 22 OCT 2016

Abstract To better understand the present and past carbon cycling and transformation processes in methane-influenced fjord and shelf areas of northern Norway, we compared two sediment cores from the Hola trough and from Ullsfjorden. We investigated (1) the organic matter composition and sedimentological characteristics to study the sources of organic carbon (C_{org}) and the factors influencing C_{org} burial, (2) pore water geochemistry to determine the contribution of organoclastic sulfate reduction and methanogenesis to total organic carbon turnover, and (3) the carbon isotopic signature of hydrocarbons to identify the carbon transformation processes and gas sources. High sedimentation and C_{org} accumulation rates in Ullsfjorden support the notion that fjords are important C_{org} sinks. The depth of the sulfate-methane-transition (SMT) in the fjord is controlled by the supply of predominantly marine organic matter to the sediment. Organoclastic sulfate reduction accounts for 60% of the total depth-integrated sulfate reduction in the fjord. In spite of the presence of ethane, propane, and butane, we suggest a purely microbial origin of light hydrocarbons in the sediments based on their low $\delta^{13}C$ values. In the Hola trough, sedimentation and C_{org} accumulation rates changed during the deglacial-to-post-glacial transition from approximately 80 cm ka^{-1} to erosion at present. Thus, C_{org} burial in this part of the shelf is presently absent. Low organic matter content in the sediment and low rates of organoclastic sulfate reduction (only 3% of total depth-integrated sulfate reduction) entail that the shallow depth of the SMT is controlled mostly by ascending thermogenic methane from deeper sources.

1. Introduction

Continental shelves and fjords play an important role in the global carbon cycle. However, due to variable primary productivity, sedimentation, and early diagenetic regimes, uncertainties in estimates of carbon fluxes for these areas remain. There is currently no consensus on the exact role of shelves and fjords in the carbon cycle, which complicates the quantification of sinks and sources and hinders the integration in global carbon cycle models [*Bauer et al.*, 2013; *Keil*, 2015; *Smith et al.*, 2015]. Shelf areas occupy only 7–10% of the global ocean area but contribute 10–30% to the global marine primary production [*Wollast*, 1991; *Bauer et al.*, 2013]. Therefore, shelf areas are important for organic carbon (C_{org}) production and carbon burial [*Berner*, 1982; *Hedges and Keil*, 1995], with a majority (>80%) of C_{org} burial in deltaic-shelf sediments near river mouths [*Berner*, 1982]. Furthermore, CO_2 air-sea exchange studies suggest that most shelves are a net sink for atmospheric CO_2 [*Cai et al.*, 2006; *Laruelle et al.*, 2010; *Chen et al.*, 2013].

A recent study by *Smith et al.* [2015] highlights the importance of fjords in C_{org} burial, estimating that 11% of annual marine carbon burial takes place in fjords although they account for only <0.1% of the marine surface area [*Keil*, 2015]. Due to a much larger area occupied by shelves than fjords, shelves still play a bigger role in total C_{org} burial (129 g C a^{-1}) than fjords (18 g C a^{-1}), but area-normalized burial rates are more than 5 times higher in fjords [*Smith et al.*, 2015]. Fjords are such "hot spots" of carbon burial because of the greater water depth compared to the adjacent sea which causes effective trapping and rapid accumulation of sediments [*Keil*, 2015].

There are several factors controlling the burial and preservation of C_{org} such as primary productivity, sediment accumulation rate, bottom water oxygenation, and organic matter source [e.g., *Hedges and Keil*, 1995].

High primary productivity can increase C_{org} burial due to a higher flux of C_{org} through the water column. A higher sedimentation rate enhances C_{org} burial [*Müller and Suess*, 1979] due to the reduced exposure time at the sediment-water interface where early diagenetic decomposition is most effective. Early diagenetic decomposition of organic matter is further reduced by low bottom water oxygen concentrations [*Hartnett et al*., 1998]. Furthermore, marine organic matter (MOM) such as fresh algal detritus is easier degradable than, for example, land-derived macromolecules like lignin, and thus less likely to be preserved [*Henrichs*, 1992].

Information about early diagenetic processes which influence the degradation and burial of C_{org}, as well as the rates of methanogenesis and methane oxidation, can be deduced from pore water geochemical profiles and inferred redox boundaries in the sediment [*Kasten et al*., 2004; *Sommer et al*., 2006; *Boetius and Wenzhöfer*, 2013; *Hong et al*., 2014b; *Hong et al*., 2016]. One of the most prominent features in sediment pore water profiles is the sulfate-methane-transition (SMT) where sulfate reduction and the anaerobic oxidation of methane (AOM) are performed by a consortium of sulfate-reducing bacteria and anaerobic methanotrophic archaea [e.g., *Hinrichs et al*., 1999; *Boetius et al*., 2000; *Orphan et al*., 2001]. Anaerobic oxidation of methane is the main microbial process preventing methane produced in marine sediments from reaching the seafloor [e.g., *Reeburgh*, 2007; *Pohlman et al*., 2013]. In most settings, the depth of the SMT is determined by (1) the content, reactivity, and burial rate of organic matter which influences sulfate consumption by organoclastic sulfate reduction [e.g., *Borowski et al*., 1999; *Riedinger et al*., 2005; *Meister et al*., 2013] and (2) by the methane flux from below [e.g., *Borowski et al*., 1996; *Bhatnagar et al*., 2008].

To better understand the present and past carbon cycling and transformation processes in methane-influenced fjord and shelf areas, we compared two sediment cores from the continental shelf offshore the Vesterålen Islands (Hola trough) and from Ullsfjorden, northern Norway. To assess C_{org} burial and sources, we analyzed the concentration of organic matter and its isotopic composition. We conducted radiocarbon (AMS-^{14}C) dating and analyses of sediment physical properties such as grain size, magnetic susceptibility, and bulk density to reconstruct sedimentation history and accumulation rates. Furthermore, we used sediment pore water profiles and transport-reaction-modeling to quantify organic matter degradation, AOM rates, and factors controlling the SMT depth in the shelf and the fjord setting. Moreover, we applied stable carbon and hydrogen isotope analyses on the gases from the sediment below the SMT to define the source of gas [e.g., *Whiticar*, 1999], and investigate the possible transformation processes of carbon in the sediment. We used δ^{13}C and δ^{2}H of methane, δ^{13}C of dissolved inorganic carbon (DIC), and δ^{13}C of ethane and propane to assess the microbial and thermogenic contribution of gases, possible hydrocarbon biodegradation, and different methanogenic pathways.

2. Study Areas

2.1. Vesterålen Shelf/Hola Trough

The continental shelf offshore the Vesterålen Islands (Figure 1), northern Norway, is relatively narrow and characterized by alternating shallow banks and deeper troughs which were formed during the last glaciations [*Bøe et al*., 2009]. The Hola trough is a cross-shelf trough, ~12 km wide, with water depths of around 200 m and high bottom current speeds. The Hola trough is confined by the banks Vesterålsgrunnen to the NE and Eggagrunnen to the SW (Figure 1b). The Norwegian Atlantic current (NAC) flows northward over the upper slope and causes sediment winnowing down to at least 500 m forming sand and gravel lag deposits, also found in the Hola trough [*Elvsborg*, 1979; *Bøe et al*., 2009]. Active methane seeps in the Hola trough were discovered in 2008 [*Chand et al*., 2008] and further investigated by *Sauer et al*. [2015] who found that the hydrocarbon gas is predominantly of thermogenic origin and most likely derived from Late Jurassic to Early Cretaceous source rocks in the region.

2.2. Ullsfjorden

Ullsfjorden is a north-south-oriented fjord in Troms County, northern Norway (Figure 1c). The fjord is ~70 km long with a maximum water depth of 285 m [*Plassen and Vorren*, 2003a]. The sediment in the fjord is largely composed of glaciomarine trough fill with thicknesses up to 200 m deposited during deglaciation [*Vorren et al*., 1989]. Ullsfjorden was deglaciated between about 15 and 11 cal ka B.P. (calibrated kilo years before 1950) [*Plassen and Vorren*, 2003b]. The Skarpnes moraine (Figure 1c) about 13 km south of the study area was dated to be 14–13.9 cal ka B.P. [*Plassen and Vorren*, 2003b] and sediment deposition in an open

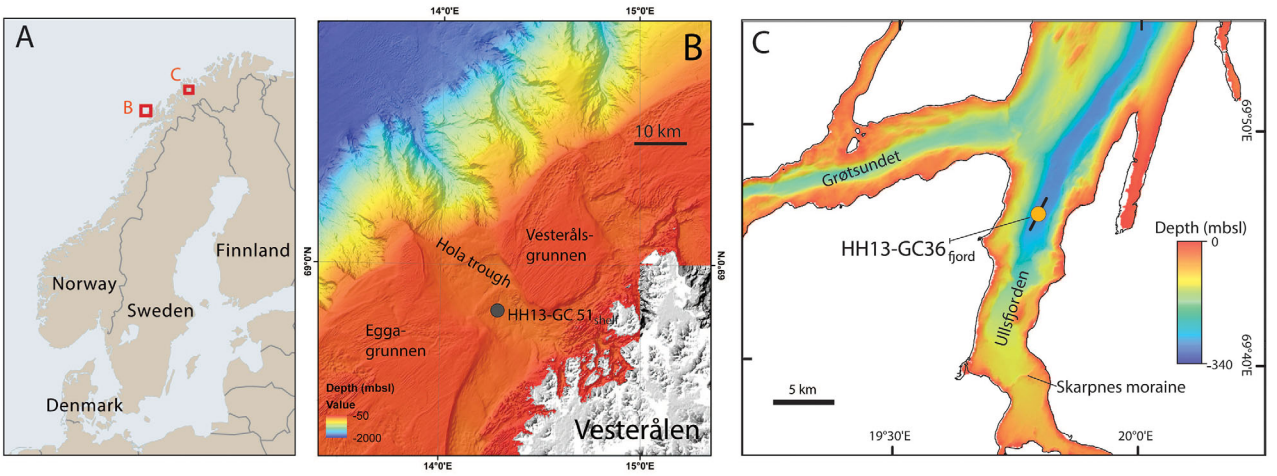

Figure 1. (a) Map of Scandinavia, (b) the Vesterålen shelf with the Hola trough and location of gravity core HH13-GC 51_{shelf}, and (c) Ullsfjorden with the location of gravity core HH13-GC 36_{fjord} and the chirp line (black line).

marine environment started around 11 cal ka B.P. [*Plassen and Vorren*, 2003b]. The postglacial sediment thickness in our study area is around 15 m (Figure 2). The bottom of Ullsfjorden is characterized by ubiquitous pockmarks [*Plassen and Vorren*, 2003a], suggested to have been formed as a result of gas escape or groundwater-related processes [*Hovland and Judd*, 1988; *Plassen and Vorren*, 2003a].

3. Material and Methods

We collected two gravity cores HH13-GC 51_{shelf} and HH13-GC 36_{fjord} (hereafter referred to as GC 51_{shelf} and GC 36_{fjord}) during a RV Helmer Hanssen cruise in April 2013. GC 51_{shelf} was retrieved from the continental shelf offshore the Vesterålen Islands at a water depth of 222 m and GC 36_{fjord} was taken from Ullsfjorden at a water depth of 276 m (Table 1 and Figure 1).

3.1. Sampling

Immediately after core retrieval, we sampled the cores for gas using the headspace technique and for pore water using the rhizon technique [*Seeberg-Elverfeldt et al.*, 2005] in intervals of 25 cm. Holes with a 3.8 mm diameter were drilled into the plastic liner with an electric drill, the rhizons were inserted with attached three-way luer lock stopcocks and 10 mL syringes to extract the pore water. After 30 min to 8 h, the syringes had filled with 10 mL of pore water.

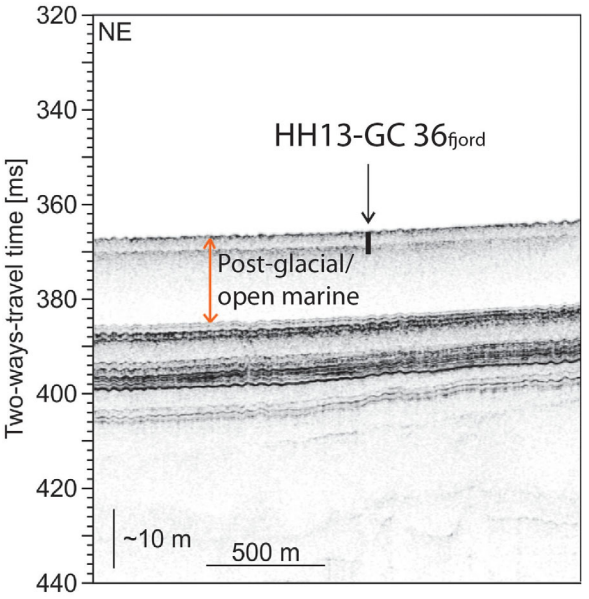

Figure 2. Chirp profile crossing the location of core HH13-GC 36_{fjord} (for location see Figure 1c).

For methane (CH_4) sampling, holes with a diameter of 1.5 cm were drilled into the plastic liner in between the rhizon holes. Three milliliter of sediment were taken using a 5 mL syringe with the luer tip removed. The sample was transferred to a 20 mL serum vial containing two glass beads and 6 mL NaOH (2.5 vol %) to prevent further microbial activity. The vial was immediately closed with a septum and an aluminum crimp seal and stored at 4°C until further analyses. The gravity cores were subsequently cut into 1 m sections and stored frozen.

Table 1. Location, Water Depth at Sampling Site, and the Recovered Length of the Two Gravity Cores GC 36_{fjord} and GC 51_{shelf}

Station Name	Latitude (N)	Longitude (E)	Water Depth (m)	Coring Device	Recovery (cm)
GC 36_{fjord}	69.7852°	19.8096°	276	Gravity corer	380
GC 51_{shelf}	68.9179°	14.2858°	222	Gravity corer	312

After thawing, the 1 m core sections were split in two halves (archive and working half) using a core splitter at the Geological Survey of Norway (NGU). Sediment samples of ~10 mL sediment were collected from the working halves in 5 cm intervals for the determination of elemental composition, grain size distribution, carbon and nitrogen content, as well as $\delta^{13}C$-C_{org}. All samples (except those for grain size analyses) were freeze dried and homogenized using a Fritsch Micro Mill PULVERISETTE 7 with agate grinding bowls and balls.

3.2. Pore Water Analyses

Dissolved phosphate (PO_4^{3-}) was determined photometrically with a Shimadzu UVmini-1240 UV-Vis Spectrophotometer using the method after *Murphy and Riley* [1962] on board RV Helmer Hanssen (error: ±0.1 μ*M*, detection limit: 0.17 μ*M*). Ammonium (NH_4^+) was detected with a flow injection teflon tape gas separator technique after *Hall and Aller* [1992] at the University of Bremen, Germany. Sulfate (SO_4^{2-}) was determined using a Dionex ICS-1100 Ion Chromatograph with a Dionex AS-DV autosampler and a Dionex IonPac AS23 column at the NGU (relative standard deviation: ±0.7%, 1σ, n = 10, standard: SPEX CertiPrep; detection limit: 0.07 m*M*). Methane concentration dissolved in the sediment pore water was analyzed by equilibrium partitioning and measured at the Swiss Federal Institute of Aquatic Science and Technology (EAWAG) using an Agilent Gas Chromatograph G1530N with a flame ionization detector. The relative standard deviation of the CH_4 measurements based on repeated measurements of a calibration standard is ±2.9% (1σ). For CH_4 concentration in the pore water, the calculated CH_4 concentration per sediment volume was corrected with an assumed constant sediment porosity of 0.8 [*Haeckel et al*., 2001].

3.3. Solid Phase Geochemistry

Analyses of total carbon (TC) and C_{org} were performed with a LECO SC-632 at the Laboratory of NGU. For TC determination, subsamples of 300–400 mg were combusted at 1350°C and the production of CO_2 determined. For C_{org} analysis, subsamples of 400–450 mg were placed in carbon-free pervious ceramic combustion boats. These were placed on a heating plate with 50°C (±5°C) and samples were treated with 10 vol % hydrochloric acid (HCl) to remove inorganic carbon (carbonate) and subsequently rinsed with distilled water and dried in the drying oven prior to analysis. Results are given in weight percentage (wt %) and the standard deviation of the TC and C_{org} measurements based on the repeated measurement of a standard was ±0.026 wt % (1σ, n = 8) and ±0.028 wt % (1σ, n = 11), respectively.

Total nitrogen (N_{tot}) was analyzed with a LECO FP 628 Nitrogen determinator at NGU. Subsamples of 200 mg were placed in tin foil and combusted to NO_x, which was transformed to N_2 and detected with a thermal conductivity cell. The standard deviation of the N_{tot} measurements based on the repeated measurement of a nitrogen standard was ±0.01 wt % (1σ, n = 11). The C/N ratio was calculated by dividing the C_{org} content (wt %) by the nitrogen content (wt %) and multiplying with 1.167 to obtain the atomic relationship.

3.4. Isotopic Analyses and Radiocarbon Dates

The stable carbon isotope composition of methane (C_1), ethane (C_2), propane (C_3), and *n*-butane (*n*-C_4), and the hydrogen isotope composition of methane were analyzed at Hydroisotop GmbH, Germany, with a GC-MS-IRMS system (Thermo Fisher Scientific GmbH). The isotopic composition is reported in ‰ (δ-values) against the international standards Vienna Pee Dee Belemnite (V-PDB) for $\delta^{13}C$ and Vienna Standard Mean Ocean Water (V-SMOW) for δ^2H. The analytical precision of $\delta^{13}C$ and δ^2H was ±1.5‰ (1σ) and ±10‰ (1σ), respectively. Methane carbon isotope composition ($\delta^{13}C$-CH_4) was also determined with a trace gas analyzer connected to a mass spectrometer (GV Instruments) at EAWAG.

The stable carbon isotopes of dissolved inorganic carbon ($\delta^{13}C$-DIC) in the pore water samples were determined with a gas bench coupled to a Delta V Plus mass spectrometer (Thermo, Switzerland) at ETH Zürich and at EAWAG using a multiflow connected to an Isoprime mass spectrometer (GV Instruments, UK). More details of the individual analyses are described in *Sauer et al*. [2015].

$\delta^{13}C$ of C_{org} was analyzed by EA-IRMS (Elemental Analyzer Isotope Ratio Mass Spectrometry) at Iso Analytical Ltd, UK. Subsamples were decarbonated with 10 vol% HCl prior to analysis with a RoboPrep-CN elemental analyzer coupled to a Europa Scientific 20-20 IRMS. Sample duplicates and reference materials were analyzed for quality control. The standard deviation (based on the reference material measurements) was $\pm 0.06‰$. All $\delta^{13}C$-DIC and $\delta^{13}C$-C_{org} data are reported relative to V-PDB.

Radiocarbon dating was carried out by accelerator mass spectrometry (AMS) at the 14Chrono Centre at the Queens University, Belfast, with a NEC compact model 0.5 MV AMS. Samples for radiocarbon analysis (foraminifera and shell fragments) were pretreated in an ultrasonic bath to remove dirt and etched with 1 vol % HCl. Subsequently, they were hydrolyzed to CO_2 using dehydrated 100% orthophosphoric acid before isotopic analysis. The calibration of ^{14}C ages was performed with clam 2.2 [*Blaauw*, 2010] using the Marine13 calibration curve [*Reimer et al*., 2013], and ages are reported in calibrated calendar years before present (cal years B.P.; present = 1950).

3.5. Sedimentological Analyses

Whole core measurements, i.e., wet bulk density (WBD) and magnetic susceptibility (MS) were conducted on the frozen gravity cores using the Standard MSCL-S core logger (GeoTek Ltd., UK) at 0.5 cm resolution with 5 s measurement time. Dry bulk density (DBD) was calculated from the WBD density following the procedure described by *Weber et al*. [1997]. C_{org} accumulation rates were calculated from linear sedimentation rates (based on the calibrated ages) and averages of DBD and C_{org} content of the sediment between each pair of ages.

MS measurements for whole cores were done with a Bartington MS2C loop sensor [*Dearing*, 1994] with 130 mm coil diameter. The MS2C loop sensor measurement produces data integrated over a distance equivalent to the sensor diameter which is symmetrically located before and behind the sensor along the core axis [*Nowaczyk*, 2002]. For control of the MS2C sensor, a certified sample piece with known magnetic susceptibility was measured. The raw MS data were processed to corrected volume-specific MS, which takes into account the relative effect of size of the core and the size of the loop sensor being used.

After lengthwise splitting and surface cleaning, core surface images were taken with the GeoScan color line-scan camera. The camera was equipped with a AF Nikkor 50 mm f/1.8D lens and three detectors using three 2048 pixel charge-coupled device (CCD) arrays for red, green, and blue light. The core surface was continuously imaged with 100 μm down and cross-core resolution. Each core section was measured with an X-rite ColorChecker as reference for basic color control.

X-ray images (XRI) of split cores were taken with the Geotek MSCL-XCT (Geotek Ltd., UK). The Geotek MSCL-XCT is equipped with a Thermo Kevex PSX10-65W X-ray source (Thermo Fisher Scientific Inc., USA) and a Varian PAXScan 2520V (Varian Medical Systems, Inc., USA) with a 1920 × 1536 pixel array as X-ray detector. The microfocal X-ray source was used with a voltage of 87 and 120 kV and a current of 125 and 140 μA for cores GC 36_{fjord} and GC 51_{shelf}, respectively. The 1 × 1 0.5pF G4 10 fps detector-CCD-mode was used for highest resolution. In the X-ray images, darker colors represent higher density.

The grain size distribution (0.4–2000 μm) was determined using a Coulter LS 200. To prevent charging and agglomeration of particles, samples were treated with 5% sodium pyrophosphate ($Na_4P_4O_7 \times 10H_2O$, MerckPA) and sonicated. Grain sizes above 2000 μm were determined by dry sieving. A duplicate of each sample was analyzed and the relative error was ±10%.

3.6. Chirp

High-resolution seismic ("chirp") data were collected with a hull-mounted Edgetech 3300-HM subbottom profiler (4 × 4 arrays). The pulse mode was 1.5–9.0 kHz, 40 ms pulse length, and a shot rate of 1 Hz.

3.7. Pore Water Modeling

We use CrunchFlow, a FORTRAN-based routine designed to simulate solute diffusion and biogeochemical reactions [*Steefel*, 2009], to investigate and quantify the biogeochemical reactions in the studied sediment cores. CrunchFlow has been applied in various cases to study the biogeochemical processes and fluid flow in ground water, geological reservoirs, and marine sediments [*Hong et al*., 2014a; *Steefel et al*., 2014, 2015; *Zhang et al*., 2015; *Hong et al*., 2016]. We simulated the concentrations of sulfate, methane, phosphate, and ammonium in pore water. We included no advection component in our modeling, as the pore water

profiles show no sign of fluid advection. We ran the simulation for 4.04 and 18 ka for station GC 36_{fjord} and GC 51_{shelf}, respectively, according to ages estimated for the base of the cores (see section 4.2). Such length of time is sufficient for the pore water system to reach steady state. Even with variable methane input, the pore water system could return to steady state in less than 5 ka. We included the following biogeochemical reactions in the model: particulate organic carbon sulfate reduction (POCSR) or also referred to as organoclastic sulfate reduction, methanogenesis (ME), and anaerobic oxidation of methane (AOM). The detailed mathematical formulation of all these reactions and essential parameters are summarized in the supporting information [*Li and Gregory*, 1974; *Berner*, 1980; *Nauhaus et al*., 2002; *Wallmann et al*., 2006; *Wegener and Boetius*, 2009; *Vavilin*, 2013; *Hong et al*., 2014b].

4. Results

4.1. Sedimentology

4.1.1. Physical Properties

The X-ray images and color photos as well as the physical properties such as WBD and MS of core GC 36_{fjord} and GC 51_{shelf} are presented in Figure 3. The sediment color of core GC 51_{shelf} varies between dark grey (2.5Y 4/1) and very dark grey (2.5Y 3/1). Three lighter intervals occur between 40 and 44, 20 and 26, and 0

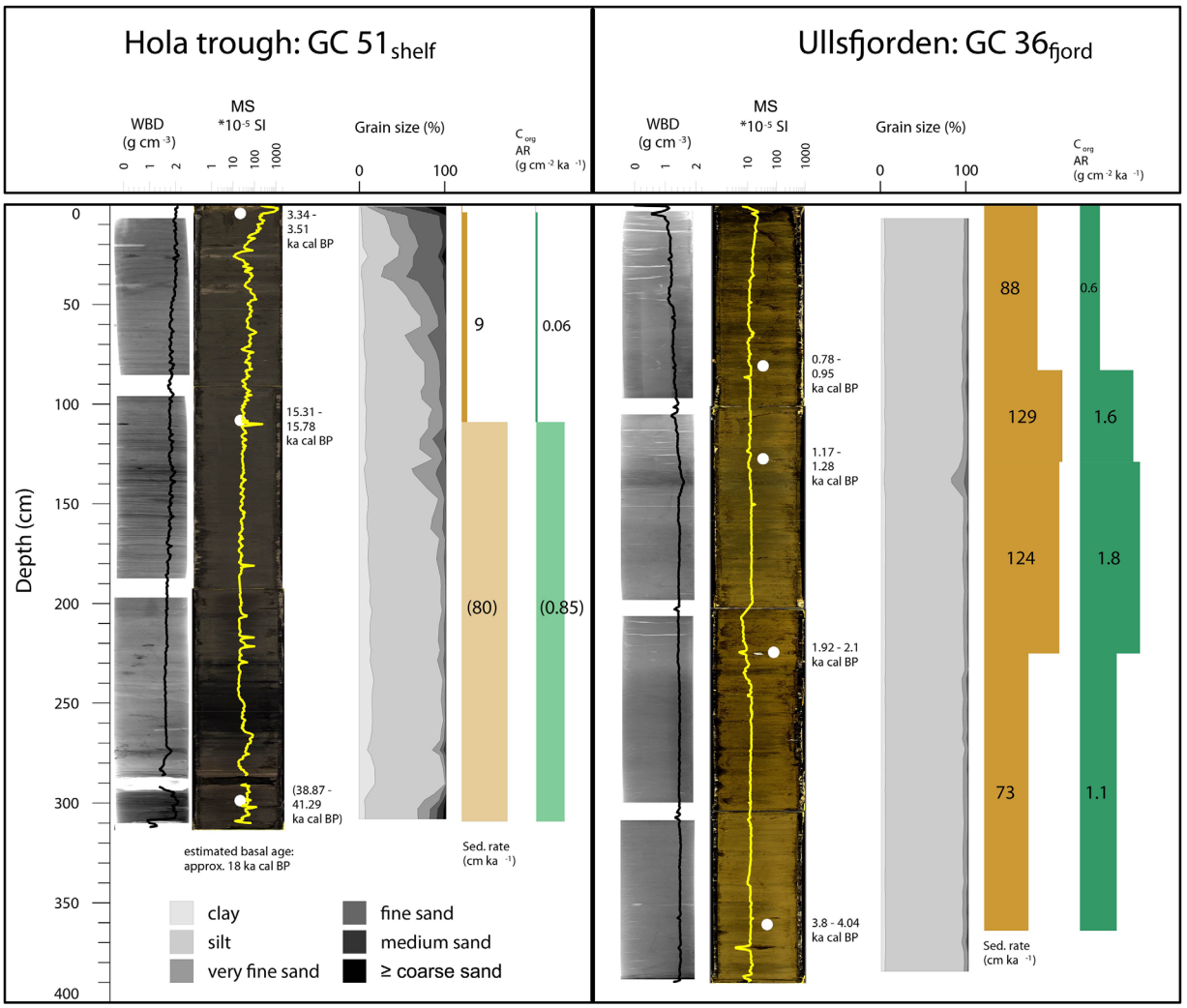

Figure 3. Sedimentological characteristics of core GC 51_{shelf} and GC 36_{fjord}: X-ray images (XRI) and color photos (stretched horizontally 400%), wet bulk density (black line on top of XRI), magnetic susceptibility (yellow line on top of color photo), calibrated ages, grain size distribution, sedimentation rate (orange), and C_{org} accumulation rate (green). Note the lighter color shading of the sedimentation rate and C_{org} accumulation rate bars below 110 cm in GC 51_{shelf} (and the rates in parentheses) indicating the uncertainty in these estimates due to the uncertain basal age.

Table 2. Results of AMS ^{14}C Dating of Different Carbonate Materials (Foraminifera and Shells) From Cores GC 36$_{fjord}$ and GC 51$_{shelf}$

					Cal Years B.P. (2σ)	
Core	Depth (cm)	Lab ID	Material	^{14}C age B.P.	Maximum	Minimum
GC 36$_{fjord}$	82–83	UBA-25349	*Thyasira granulosa*	1,333 ± 34	948	784
	128–129	UBA-25350	*Musculus niger*	1,665 ± 26	1,282	1,170
	224–225	UBA-25351	*Thyasira granulosa*	2,377 ± 28	2,101	1,916
	363–364	UBA-25352	*Thyasira granulosa*	3,920 ± 37	4,044	3,802
GC 51$_{shelf}$	3–4	UBA-21635	Mixed benthic and planktonic foraminifera	3,537 ± 30	3,513	3,344
	108–109	UBA-21636	Shell fragment	13,406 ± 59	15,780	15,310
	299.5–300.5	UBA-21637	Mixed benthic and planktonic foraminifera	35,865 ± 596	41,290	38,870

and 4 cm. The lowermost 20 cm of the core are coarse grained with on average 26% of the >63 μm fraction (sand and coarser). A marked fining occurs around 290 cm with increases in the clay and silt fraction (Figure 3). Between 290 and 170 cm the grain size distribution is relatively constant (13.5% clay, 80% silt, and 6.5% sand and coarser). A gradual coarsening occurs in the uppermost ca. 170 cm. Silt content decreases from 80% at 170 cm to 7% at 1 cm depth, whereas the >63 μm fraction increases from 8% to 91% in the same interval. In accordance with grain size, MS is highest at the top of the core. Below 100 cm, MS is on average 30 × 10^{-5} SI (Figure 3). Between 100 and 10 cm depth MS is on average 60 × 10^{-5} SI and at 2 cm sediment depth MS values reach up to 1200 × 10^{-5} SI. The WBD below 290 cm is approximately 2 g cm^{-3}. At 290 cm, there is a density drop to 1.5 g cm^{-3} coinciding with the marked fining of the sediment. The density increases gradually from ~1.5 g cm^{-3} at 290 cm to 2 g cm^{-3} at the top of the core. The X-ray images of core GC 51$_{shelf}$ reveal several larger clasts in the lowermost 10 cm of the core and a distinct lamination from 200 to 80 cm.

The sediment color of core GC 36$_{fjord}$ varies between olive (5Y 4/4) and olive grey (5Y 4/2). The grain size distribution is constant throughout the core with a silt content of 89% and on average 6% of the <63 μm fraction. The only exception is the interval at 137–140 cm depth where silt content decreases to 77% and an increase in the >63 μm fraction up to 19% can be observed (Figure 3). MS is lower throughout GC 36$_{fjord}$ (average is 13 × 10^{-5} SI) compared to GC 51$_{shelf}$. WBD is on average 1.46 g cm^{-3} in the lowermost 250 cm of the core and decreases down to 1 g cm^{-3} toward the top of the core in the uppermost 130 cm. Only the interval with coarser grain sizes has a higher density of 1.6 g cm^{-3} (Figure 3). The X-ray images show a homogenous core without any lamination. The only feature is a darker shade of the coarser, denser interval at 137–140 cm.

4.2. Chronology and Sedimentation Rates

We obtained three ^{14}C ages from core GC 51$_{shelf}$ and four from GC 36$_{fjord}$ (Table 2). In core GC 36$_{fjord}$, we expect the top of the core to represent present sedimentation. The sample closest to the bottom of the core was dated to between 3802 and 4044 cal years B.P. The uppermost sample of core GC 51$_{shelf}$ (3–4 cm) gave an age between 3344 and 3513 cal years B.P. The sample at 300 cm sediment depth GC 51$_{shelf}$, consisting of a mixture of benthic and planktonic foraminifera, was dated to be between 38,870 and 41,290 cal years B.P with an error of ±596 years. We suspect that this is not the actual depositional age of the sediment, but the age of foraminifera redeposited from older strata.

Average sedimentation rates calculated between each pair of ^{14}C dates vary between 73–129 cm ka^{-1} in core GC 36$_{fjord}$ (Figure 3). For core GC 51$_{shelf}$, the sedimentation rate between the upper two ^{14}C dates was 9 cm ka^{-1}, which is around a magnitude lower than that in core GC 36$_{fjord}$. We disregarded the lowest ^{14}C age in core GC 51$_{shelf}$ and instead estimated the age of the sediment interval to be 18 cal ka B.P. The latter is based on the sedimentology of the core with a basal till/glacimarine diamicton in the lowermost part, which was likely deposited between 17.5 and 18 cal ka B.P. according to the reconstruction of glacier retreat on the shelf offshore the Vesterålen Islands by *Vorren et al*. [2015]. This interpretation is based on the high abundance of angular large clasts, high density and the absence of layering [*Forwick and Vorren*, 2009] in the lower 5 cm of the core. According to this age model, the average sedimentation rate is 80 cm ka^{-1} for the lowermost 2 m of core GC 51$_{shelf}$ (Figure 3).

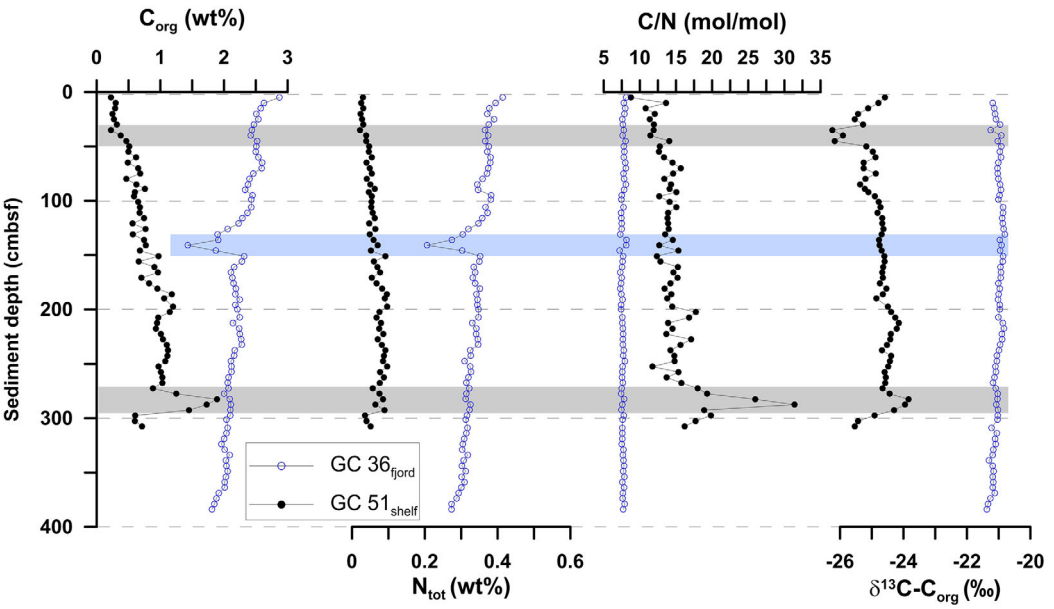

Figure 4. Profiles of C_{org} content, total nitrogen content (N_{tot}), the atomic C/N ratio, and $\delta^{13}C$-C_{org} values of sediment core GC 36_{fjord} (blue empty circles) and GC 51_{shelf} (black filled circles). The sediment depth is given in cm below seafloor (cmbsf). The grey shaded areas mark intervals of core GC 51_{shelf} where pronounced changes in $\delta^{13}C$-C_{org} values and/or C/N ratio are observed. The blue shaded area marks an interval of presumably redeposited sediment in GC 36_{fjord}.

4.3. Organic Sediment Geochemistry

The C_{org} content in the lowermost 10 cm of GC 51_{shelf} is around 0.6 wt % (Figure 4). At 282 cm, there is a peak in C_{org} up to 1.9 wt % and then a steady decrease from 1 wt % at 270 cm to 0.2 wt % at 5 cm depth. The total nitrogen content (N_{tot}) of the sediment decreases slightly upward through the core from 0.09 wt % to 0.03 wt % (average: 0.06 wt %, n = 62). The C/N ratio shows a peak at 288 cm of 31, coinciding with the peak in C_{org} content. From 270 cm to the top of the core, the C/N ratio decreases from ~18 to ~9. The average C/N ratio of core GC 51_{shelf} is 14.8 ± 3.3. The average $\delta^{13}C$-C_{org} value of core GC 51_{shelf} is $-24.8‰$ ($\pm 0.47‰$, n = 62). In the interval between 288 and 283 cm, the $\delta^{13}C$-C_{org} values are higher (around $-23.9‰$), and between 45 and 35 cm, the $\delta^{13}C$-C_{org} values are lower than the average (around $-26‰$).

C_{org} content of GC 36_{fjord} is 1.8 wt % at the bottom of the core and increases steadily to 2.9 wt % at 5 cm depth, interrupted by a sharp drop to 1.4 wt % at 141 cm depth (Figure 4, blue band). The N_{tot} content increases gradually from 0.27 wt % at the bottom of the core to 0.4 wt % at 5 cm depth with one negative excursion to 0.2 wt % at 140 cm depth, showing the same pattern as the C_{org} content. The atomic C/N ratio is constant throughout the core with an average of 7.7 ± 0.2. The $\delta^{13}C$-C_{org} values also show little variation throughout the core with an average of $-21.04‰ \pm 0.14‰$.

4.4. Pore Water Geochemistry

We analyzed 16 pore water samples from GC 36_{fjord} for their dissolved constituents and the isotopic composition of DIC, and 15 samples (sediment + pore water) for the headspace methane concentration and methane carbon isotopes (Table 3). These data were plotted and compared to pore water data of core GC 51_{shelf} (Figure 5) from a seep setting in the Hola trough which was described in detail by *Sauer et al.* [2015].

In core GC 36_{fjord}, sulfate concentrations decreased downward and are below detection limit at 162 cm depth. Methane concentrations were below 0.2 m*M* in the upper 125 cm of the sediment core and then increased to a maximum of 7.6 m*M* at 325 cm (Table 3). Thus, the SMT spanned an interval from 125 to 162 cm sediment depth. The SMT depth in GC 51_{shelf} was between 80 and 110 cm [*Sauer et al.*, 2015]. Pore water concentrations of ammonium and phosphate increased with depth in core GC 36_{fjord} to values up to 7.6 m*M* and 299 μ*M*, respectively, at the base of the core. Ammonium concentrations at the base of the core are more than 24 times higher in GC 36_{fjord} compared to GC 51_{shelf} [*Sauer et al.*, 2015]. Phosphate concentration was also significantly higher in core GC 36_{fjord} than GC 51_{shelf}.

Table 3. Results of Pore Water Analyses of Core GC 36_{fjord}

Depth (cmbsf)	SO_4^{2-} (m*M*)	PO_4^{3-} (μ*M*)	NH_4^+ (m*M*)	δ^{13}C-DIC (‰ V-PDB)	Depth (cmbsf)	CH_4 (m*M*)	δ^{13}C-CH_4 (‰ V-PDB)
11	25.2	37.1	0.5	−11.9	25	0.0	
36	20.4	55.3	1.4	−9.8	50	0.1	
62	13.8	92.5	2.2	−18.4	75	0.1	
89	9.9	82.9	2.8	−18.7	100	0.1	
113	6.5	88.2	3.3	−19.2	125	0.2	−85.3
138	3.0	146.8	3.9	−17.9	150	0.3	−91.0
162	<0.07	161.1	4.2	−18.4	175	1.0	
188	<0.07	167.8	4.6	−15.5	200	2.7	−96.5
213	<0.07	191.7	5.1	−8.9	225	4.0	−94.9
238	<0.07	212.7	5.8	−8.6	250	6.5	−94.9
264	<0.07	228.9	6.0	−6.3	275	5.7	−93.9
289	<0.07	236.6	6.3	−5.5	300	6.9	−92.3
314	<0.07	266.2	6.7	−2.6	325	7.6	−91.8
339	<0.07	272.9	7.0	−2.8	350	5.9	−89.6
359	<0.07	279.4	7.1	−1.9	365	5.3	−89.5
374	<0.07	298.7	7.6	−1.2			

The δ^{13}C-CH_4 of GC 36_{fjord} ranged from −96.5‰ to −85.3‰ (Table 3). The lowest value was at 200 cm depth and values increased upward through the SMT to −85.3‰ and downward as well to −89.5‰. In comparison, δ^{13}C-CH_4 values in GC 51_{shelf} were around 30‰ higher than in GC 36_{fjord} and ranged between −60‰ and −53‰ (Figure 5).

In GC 36_{fjord}, the lowest values of δ^{13}C-DIC (between −19.2‰ and −17.9‰) were found in the interval from 62 to 162 cm. Below the SMT, δ^{13}C-DIC values increased up to −1.2‰ and above the SMT to roughly −10‰ (Table 3). In GC 51_{shelf}, the lowest δ^{13}C-DIC value was −12‰. The same increasing trend as in GC 36_{fjord} is observed below the SMT in GC 51_{shelf}, but δ^{13}C-DIC increased stronger with depth to a value of up to +18‰ in GC 51_{shelf} (Figure 5).

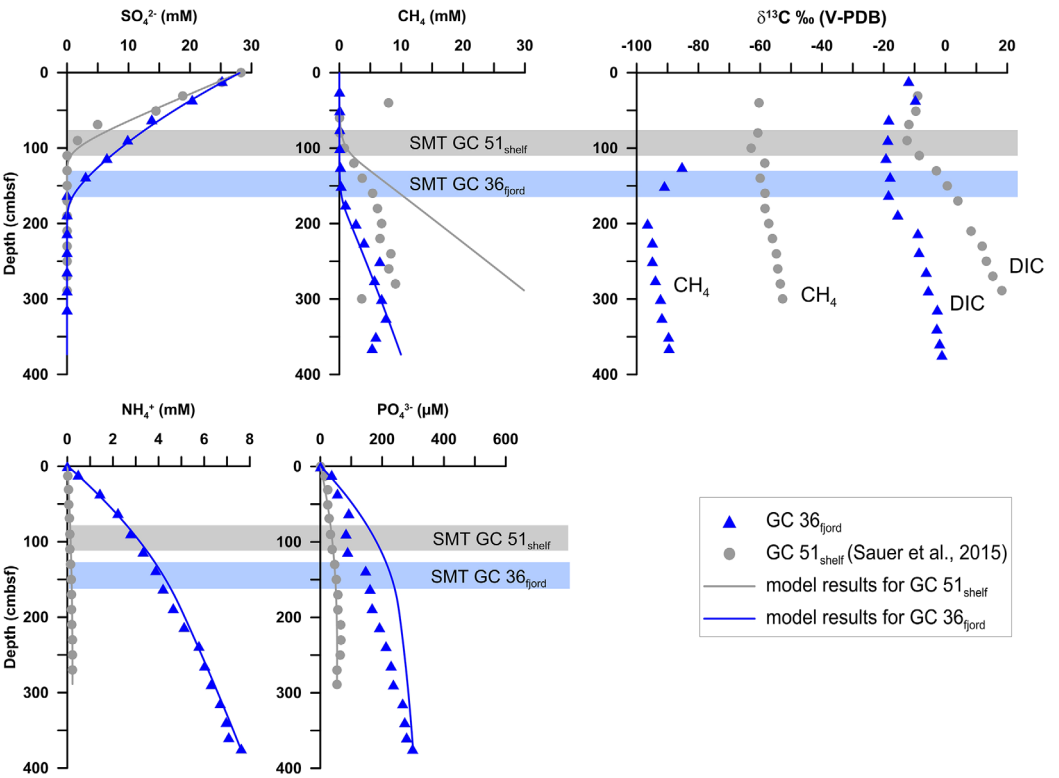

Figure 5. Pore water concentration profiles in core GC 36_{fjord} from Ullsfjorden (blue triangle) and previously published data from GC 51_{shelf} from the Hola trough (grey dots) [*Sauer et al.*, 2015]. The lines represent the fitted model results for both cores. The grey (blue) bars represent the sulfate-methane-transition in core GC 51_{shelf} (GC 36_{fjord}).

Table 4. Results of Isotopic Analyses of Methane, Ethane, Propane, and Butane of GC 36_{fjord} and GC 51_{shelf}[a]

	δ^2H (‰ V-SMOW)	δ^{13}C (‰ V-PDB)			
Sample	CH_4	CH_4 (C_1)	C_2H_6 (C_2)	C_3H_8 (C_3)	nC_4H_{10} (n-C_4)
GC 36–200 cm	−218	−96.5		−37.3	−36.4
GC 36–365 cm	−220	−89.5	−57.1	−38.6	−33.7
GC 51–140 cm	−218	−60.0	−34.4	−14.9	−22.4
GC 51–220 cm	−225	−56.1	−36.5	−16	−22.5
GC 51–300 cm	−223	−52.7	−34.4	−12.1	−24.8

[a]All values of GC 51_{shelf} are from the study of *Sauer et al*. [2015].

In general, our pore water model can satisfactorily fit the observed profiles except for the methane concentration profiles for both sites, and the phosphate concentration profile at GC 36_{fjord} (Figure 5). Results of methane concentration were potentially affected by degassing during core recovery [*Dickens et al*., 2003]. These measurements are therefore only minimum constraints of in situ methane concentrations. The higher phosphate concentration at GC 36_{fjord} estimated by our model compared to the observation may be caused by the adsorption of phosphate onto Fe(oxyhydr)oxides [*Krom and Berner*, 1980] lowering the dissolved phosphate concentration in the measured pore water data.

4.5. Gas Isotopes

We analyzed two samples of core GC 36_{fjord} (200 and 365 cm sediment depth) for δ^2H of methane and the δ^{13}C of ethane, propane, and butane. In both samples, the δ^2H-CH_4 was very similar, −218‰ and −220‰ (Table 4). The δ^{13}C of the higher molecular weight hydrocarbons increased with increasing carbon number: methane (−96.5‰ to −89.5‰), ethane (−57.1‰), propane (−38.6‰ to −37.3‰), and *n*-butane (−36.4‰ to −33.7‰). In GC 51_{shelf}, δ^2H-CH_4 values [*Sauer et al*., 2015] were similar to those in GC 36_{fjord}. However, the δ^{13}C values of ethane, propane, and *n*-butane were higher in GC 51_{shelf} by between 11‰ and 23‰.

5. Discussion

5.1. Organic Matter Source

We consider three possible sources of the sedimentary organic matter in the studied gravity cores: marine organic matter (MOM), fresh terrestrial organic matter (TOM), and fossil organic matter from weathered or glacially eroded bedrock [*Tyson*, 1995]. For a first-order discrimination between MOM and TOM, we use the $\delta^{13}C$-C_{org} and the C/N ratio [e.g., *Meyers*, 1994; *Hall and McCave*, 1998; *Schubert and Calvert*, 2001; *St-Onge and Hillaire-Marcel*, 2001; *Knies et al*., 2003; *Knies and Martinez*, 2009; *Yu et al*., 2010]. Marine algae typically have atomic C/N ratios between 4 and 10, mostly exhibiting the "Redfield" carbon to nitrogen ratio of 7 [*Meyers*, 1994]. Generally, in freshly deposited sediments, this value is slightly higher (9–10) due to the preferential loss of nitrogen during organic matter degradation in the water column [*Fenchel et al*., 2012b]. In contrast, the C/N ratio of vascular land plants is $\geq$20 [*Meyers*, 1994].

The δ^{13}C value of TOM is generally lighter than that of MOM. For the δ^{13}C of TOM, one has to differentiate between C3 and C4 plants, because they discriminate differently against $^{13}CO_2$ [*Farquhar et al*., 1989]. However, at high latitudes, the influence of C4 plants is minor [e.g., *Teeri and Stowe*, 1976]. TOM derived from C3 plants has δ^{13}C values that commonly range between −23‰ and −35‰ with an average of −27‰ [*Meyers*, 1994], whereas MOM normally shows heavier isotopic values between −13‰ and −31‰ [*Tyson*, 1995]. *Rau et al*. [1982] found an average δ^{13}C value of −20.9‰ for marine phytoplankton at latitudes higher than 62°N and *Knies et al*. [2003] reported a very similar value of −20.3‰ for northern Norwegian coastal MOM.

The sedimentary organic matter in Ullsfjorden is dominated by marine phytoplankton as the average $\delta^{13}C$-C_{org} in core GC 36_{fjord} of −21‰ (Figure 6) coincides very well with the values found for high northern latitude marine phytoplankton [*Rau et al*., 1982; *Schubert and Calvert*, 2001]. Also, the average C/N ratio (7.7) falls well within the MOM range (Figure 6). The vegetation cover of the hinterland seems to play a minor role in supplying organic matter to Ullsfjorden. This is further supported by the constantly low MS, which commonly suggests a dominance in marine biogenic material in the sediment [e.g., *Hounslow and Maher*, 1999] (Figure 3). Since there is no significant variation in the $\delta^{13}C$-C_{org} and C/N ratio within GC 36_{fjord}

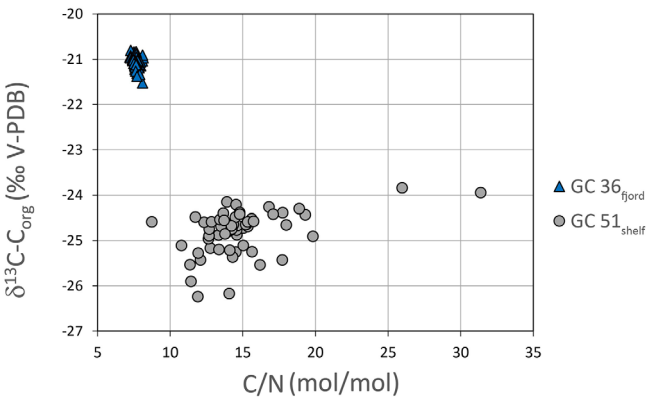

Figure 6. Plot of sedimentary δ^{13}C-C_{org} against C/N ratio of cores GC 36_{fjord} (blue triangles) and GC 51_{shelf} (grey dots).

(Figures 4 and 6), the organic matter source has probably stayed constant over the last approximately 4000 years.

In contrast, the sedimentary organic matter of core GC 51_{shelf} shows a much stronger terrestrial influence with a higher average C/N value of 14.8 and lower δ^{13}C values of on average $-24.8‰$ (Figure 6). Moreover, there is considerably more variation in both C/N ratios and δ^{13}C values in GC 51_{shelf} than in GC 36_{fjord} suggesting changes in the organic matter source over time. Yet we found no correlation between the C/N ratio and δ^{13}C-C_{org} values in core GC 51_{shelf} ($r^2 < 0.2$) which points to a mixing of more than two end members with different δ^{13}C and C/N signatures. The poor correlation and the lack of well-constrained end members make a quantification of the different C_{org} sources in GC 51_{shelf} difficult.

Besides the common organic matter sources considered, there are two intervals in GC 51_{shelf} that demonstrate abnormal geochemical signatures which may reflect organic matter from less common sources (Figure 4, grey bands). These two intervals with the most prominent changes in δ^{13}C and/or C/N in core GC 51_{shelf} are 35–45 cm (drop in δ^{13}C-C_{org} to $-26‰$) and 282–292 cm (increase in C/N ratio to 31 and in δ^{13}C-C_{org} to $-24‰$). The latter depth interval also corresponds to a peak in C_{org} content of up to 1.9 wt % (Figure 4). The first interval could be explained by either an increased proportion of TOM (assumed average $-27‰$), or a contribution of methanogenic/methanotrophic microbial biomass which can be very depleted in δ^{13}C with values up to $-120‰$ of some archaeal lipids [*Yoshinaga et al*., 2015]. *Yoshinaga et al*. [2015] reported, for example, a substantial contribution of AOM-related biomass to C_{org} in sediment cores from cold seep sites off Pakistan resulting in bulk δ^{13}C-C_{org} values as low as $-42‰$. The Hola trough also hosts cold seeps with high methane fluxes that can promote microbial methanotrophic activity [*Sauer et al*., 2015]. In core GC 51_{shelf}, several intervals of authigenic methane-derived carbonate nodules tracking past SMTs were reported above the present SMT (corresponding to the light intervals mentioned in the core description), with the largest nodules found in the interval between 40 and 44 cm and δ^{13}C-carbonate values of $-12‰$ [*Sauer*, 2016], suggesting shallower SMT depths in the past. Given the carbonate evidence for AOM within the upper part of GC 51_{shelf}, the occurrence of strongly ^{13}C-depleted methanotrophic biomass is possible. Thus, a contribution of methanotrophic biomass to the sedimentary organic matter may be responsible for the lighter δ^{13}C-C_{org} values in the upper interval of core GC 51_{shelf} (Figure 4) between 35 and 45 cm. Furthermore, there is no increase in C/N ratio in this interval, which would be expected if an increased TOM proportion was responsible for lighter δ^{13}C values. Bacterial biomass has a C/N ratio of around 5 [*Fenchel et al*., 2012a], so it cannot be distinguished from MOM based on the C/N ratio.

For the second interval (282–292 cm), elevated C/N values of up to 31 would normally be interpreted to indicate high input of TOM at that time. However, the δ^{13}C-C_{org} values do not support this interpretation. The heavier isotopic values of up to $-23.8‰$ indicate lower terrestrial organic matter input compared to the rest of the core. A possible explanation might be an interval dominated by fossil organic matter derived from the erosion of organic-matter-rich bedrock in the vicinity. The C/N ratio usually increases with progressive decomposition of the organic matter due to the preferential removal of nitrogen by the degradation of high-N compounds during diagenesis [*Fenchel et al*., 1998; *Lehmann et al*., 2002]. Thus, old organic matter should have higher C/N ratios. Late Jurassic to Early Cretaceous rocks with high organic carbon contents were drilled about 30 km away from the present study area on the shelf and were found at only 10 m depth below the seafloor [*Hansen et al*., 1992; *Smelror et al*., 2001]. Furthermore, C/N ratios of the same formation in the Barents Sea were found to vary between 20 and 50 [*Langrock*, 2004] and are thus similar to the values we find in the high-C_{org} interval of GC 51_{shelf}. Thus, if these rocks outcrop in the vicinity of our study area they could have provided Late Jurassic to Early Cretaceous organic matter with high C/N ratios to the shelf,

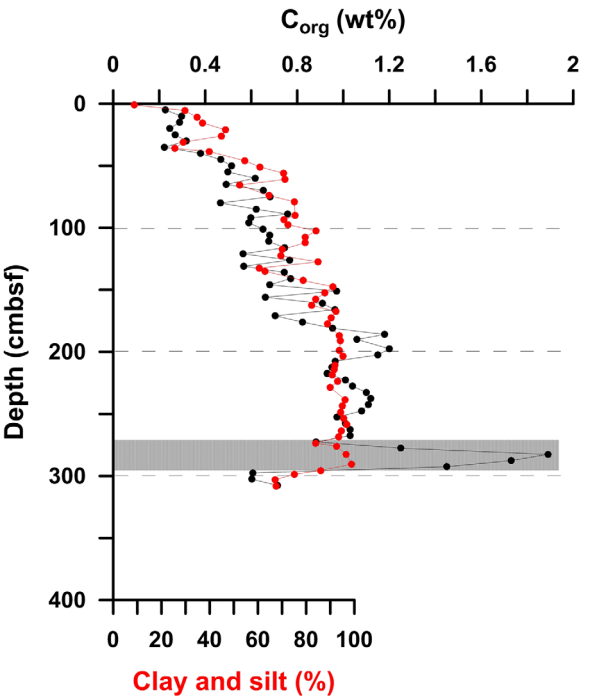

Figure 7. Comparison of C_{org} content and the sum of the clay and silt fraction of GC 51_{shelf}. The shaded band represents an interval with high C_{org} content, which is an exception to the correlation between grain size distribution and C_{org} content.

most likely by glacial erosion. As most of the core GC 51_{shelf} represents sedimentation in a dynamic glacial to post glacial environment with contribution of sediment from glacial erosion of the hinterland we consider ancient eroded C_{org} in this interval of GC 51_{shelf} as a likely source.

5.2. Organic Matter Burial and Sediment Characteristics

Core GC 36_{fjord} comprises a massive mud deposited in an open marine environment during the last ~4000 years. The grain size distribution remains rather constant except for a thin interval at 140 cm (Figure 3). This interval shows a higher fraction of coarse-grained material, higher density, lower C_{org} and N_{tot} content (Figure 4, blue band). This can be explained by a higher proportion of clastic material with higher density and coarse grain size in this interval which dilutes the marine components. We assume that this interval is composed of reworked sediments. Other than the local minima in C_{org} content at 140 cm, GC 36_{fjord} shows a regular C_{org} profile with decreasing concentration with depth likely due to early diagenetic degradation [*Hedges and Keil*, 1995]. The constant C/N ratio shows that there is no preferential nitrogen removal during early diagenesis in these sediments, as opposed to observations in the water column [*Fenchel et al.*, 2012b]. Despite a decreasing C_{org} content with depth, the overall C_{org} content is high (average $>$ 2 wt %).

In comparison, the C_{org} content in GC 51_{shelf} is generally low but increases gradually with depth. The C_{org} profile of GC 51_{shelf} correlates with grain size distribution (Figure 7): the C_{org} content increases with depth along with the increase in the fine fraction, except for the interval 282–292 cm with a C_{org} peak. We assume that the organic matter in the sediment is associated with the fine grained fraction [*de Haas et al.*, 2002]. This is supported by findings of *Bianchi and Bauer* [2011] that 90% of river and estuarine-derived organic carbon entering the coastal zone is associated with mineral matrices in organo-clay aggregates.

The decrease in the fine fraction toward the top of the core might be a result of increased erosion by strong bottom currents in the Hola trough since the deglaciation [*Bøe et al.*, 2015]. An increase in current velocity has also been hypothesized for Malangsdjupet (a cross-shelf trough north of the Hola trough) during the Holocene due to changes in marine currents along the coast [*Elvsborg*, 1979]. The establishment of modern oceanographic conditions in the Nordic Sea with the NAC and the Norwegian Coastal Current (NCC) eroding and winnowing fine material and leaving a lag deposit of sand, gravel, and boulders on the shelf probably started around the Bølling Allerød interstadial [*Bøe et al.*, 2015, and references therein]. The typical Quaternary succession on northern Norwegian shelves includes basal tills and glaciomarine sediments [*Vorren et al.*, 1989] that discordantly overlie Cretaceous sedimentary rocks. The lowermost 12 cm of GC 51_{shelf} is poorly sorted (Figure 3) with some angular clasts up to 2 cm in diameter (Figure 8) suggesting a glacial origin, either a basal till or glaciomarine sediment [*Elvsborg*, 1979; *Forwick and Vorren*, 2009].

The ^{14}C age determined on the foraminifera at 300 cm (around 40 cal ka B.P.) does not represent the actual depositional age, because the foraminifera are probably redeposited from older marine sediment. We estimated the base of the core to be the age of the till which deposited when the ice retreated from this area. This was estimated to be around 18–17.5 cal ka B.P. by *Vorren et al.* [2015], who ascribed a grounding zone wedge just next to the core site GC 51_{shelf} to the Flesen event dated to ~14.5 ^{14}C ka/17.5 cal ka B.P. [*Vorren*

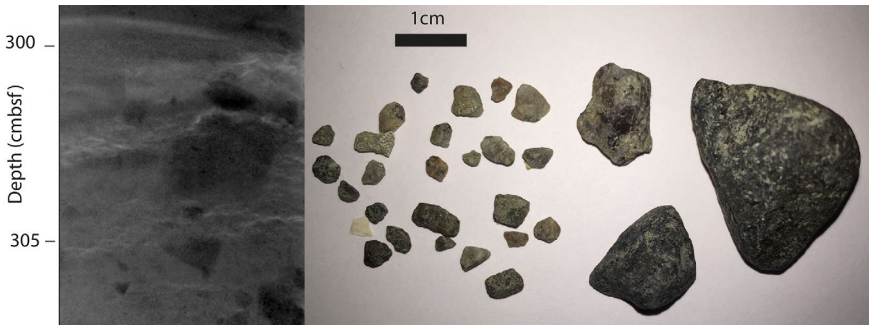

Figure 8. (left) X-ray image of the lower part of GC 51_{shelf} and (right) photo of the grains > 2 mm contained in this section.

and Plassen, 2002]. Laminated finer grained material covering the till from 200 to 80 cm in core GC 51_{shelf} was probably deposited from sediment-laden meltwater plumes during deglaciation [*Vorren et al*., 1984]. Compared to present current strength, the strength of the along-slope current was generally lower during the glacial [e.g., *Laberg et al*., 2005] allowing the deposition of finer grained material. Furthermore, the sedimentation rate was much higher because of the proximity of the glacier front representing an important sediment source. Since postglacial times, the dominant erosional process in this area is the winnowing along the shelf and upper slope by the NAC [*Vorren et al*., 1984; *Laberg et al*., 2005; *Bellec et al*., 2012]. Present estimates of bottom current speed are up to 0.7 m s^{-1} [*Bøe et al*., 2009]. At this speed, pebbles up to 3 mm in diameter can be eroded and boulders transported as bedload [*Johnson et al*., 1982]. This formed a lag deposit, which resulted in the pebbly sand we observed as the very top layer in the Hola trough.

Foraminifera from 3 to 4 cm sediment depth were dated to be around 3.5 cal ka B.P., which supports the notion that the surface sediments were eroded. We also suggest that C_{org} burial in this area is presently absent. Any MOM from primary production is probably remineralized in the water column or transported off the shelf toward the shelf break and further downslope along with the fine-grained sediment fraction [*de Haas et al*., 2002; *Bøe et al*., 2015].

Based on the profiles of C_{org} content and grain size distribution (Figure 7), we suggest that there has been a progressive decrease in the deposition of fine-grained sediments and associated organic matter during the last 15 ka. The shelf area apparently played a more important role in C_{org} burial during the last glacial than during the present interglacial. Similar findings of glacial-interglacial variations of C_{org} burial have been observed in other areas along the NW European continental slope [*Hall and McCave*, 1998]. The C_{org} deposition on the slope has decreased in the past 20 ka to less than half, from late glacial to Holocene values: from 0.06 g C cm^{-2} ka^{-1} to less than 0.03 g C cm^{-2} ka^{-1} [*Hall and McCave*, 1998].

Our C_{org} accumulation rates estimated for Ullsfjorden (0.6–1.8 g C cm^{-2} $ka^{-1,}$ Table 5) are similar to those from other high northern latitude fjords. In Storfjorden (Spitsbergen) and the Saguenay fjord (Quebec), C_{org} accumulation rates are between 1.2 and 4 g C cm^{-2} ka^{-1} [*Winkelmann and Knies*, 2005] and around 3 g C cm^{-2} ka^{-1} [*St-Onge and Hillaire-Marcel*, 2001]. A recent paper by *Smith et al*. [2015] further highlights the role of fjords as a global C_{org} sink. They report a global average C_{org} accumulation rate for fjords of 5.4 g C cm^{-2} ka^{-1} and that 11% of annual marine carbon is buried in fjord sediments. The C_{org}

Table 5. Average Values of Sedimentation Rate (SR), Dry Bulk Density (DBD), and C_{org} Content Used To Calculate C_{org} Accumulation Rate (AR)[a]

Core	Interval (cm)	Approximate Time Interval (cal years B.P.)	SR (cm ka^{-1})	DBD (g cm^{-3})	Average Corg (%)	Bulk AR (g cm^{-2} ka^{-1})	Corg AR (gC cm^{-2} ka^{-1})
GC 36_{fjord}	0–82.5	Present to 875	88	0.28	2.54	24.50	0.621
	82.5–128	875–1231	129	0.54	2.29	69.32	1.585
	128–225	1,231–2,005	124	0.69	2.13	85.40	1.821
	225–364	2,005–3,905	73	0.70	2.07	51.45	1.066
	0–364	Present to 3,905	92	0.6	2.2	55.20	1.214
GC 51_{shelf}	3.5–108.5	3,481–15,613	8.7	1.38	0.48	12.01	0.058
	108.5–312	15,613–18,000	80	1.10	0.96	88.00	0.845

[a]The intervals are determined by the depths of ^{14}C dating.

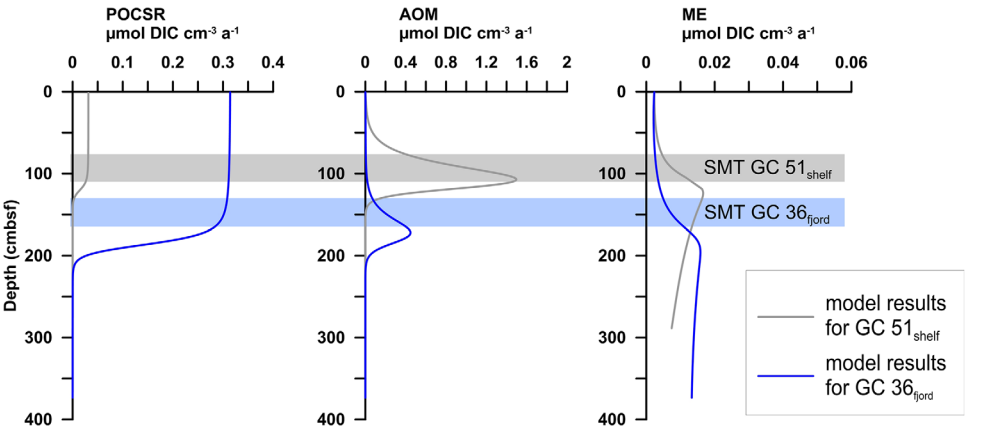

Figure 9. Modeled rates of anaerobic oxidation of methane (AOM), methanogenesis (ME), and particulate organic carbon sulfate reduction (POCSR) at sites GC 36_{fjord} and GC 51_{shelf}.

accumulation rate that we estimated for Ullsfjorden lies at the lower end of C_{org} accumulation rates that *Smith et al*. [2015] determined for fjords worldwide, but it is still multiple times higher than accumulation rates determined for site GC 51_{shelf} located on the shelf in the Hola trough.

5.3. Biogeochemical Reactions in the Sediments: Sulfate Reduction, Methanogenesis, and AOM

In order to quantify the degradation of organic matter in shelf and fjord sediments by particulate organic carbon sulfate reduction (POCSR) and methanogenesis (ME), we applied a transport-reaction model to the key pore water profiles (Figure 5). By fitting sulfate, ammonium, and phosphate profiles, we are able to estimate the overall organic matter degradation rate by the two reactions. Our model reveals an order of magnitude higher POCSR rate for GC 36_{fjord} than for GC 51_{shelf} and slightly higher ME rates at the GC 36_{fjord} site (Figure 9 and Table 6). The high organic matter degradation rate at GC 36_{fjord} is potentially fueled by the high input of labile MOM at this site as suggested by its sediment geochemistry (C_{org} content, C/N ratio, and $\delta^{13}C$-C_{org} values) (Figure 4) and the higher accumulation rate of C_{org} (Table 5).

The overall depth-integrated rates of sulfate reduction are in the same range at both sites: 47.5 µmol SO_4 cm^{-2} a^{-1} (GC 36_{fjord}) and 58.1 µmol SO_4 cm^{-2} a^{-1} (GC 51_{shelf}). In a global study of sulfate reduction rates, *Bowles et al*. [2014] found highest average rates in inner shelf environments of 39 cm^{-2} a^{-1}, which is the same order of magnitude as our sulfate reduction rates. Although the total depth-integrated rates of sulfate reduction are similar at our shelf and fjord site, the processes governing the sulfate pore water profiles are different. Even though the organic matter burial and decomposition rates are significantly higher in GC 36_{fjord}, we observed a shallower SMT in GC 51_{shelf}. Our model results suggest that 97% of the depth-integrated sulfate reduction at GC 51_{shelf} is mediated by AOM (Table 6) indicating a strong methane influence at this site. Methane that is utilized during AOM can be produced by organic matter degradation via in situ ME or supplied from sources deeper than the depth we considered in the model (the core length). Our model estimated that only 4.3% of the methane carbon is produced by in situ ME at GC 51_{shelf} (Table 6). Thus, most of the methane that contributes to AOM at this site comes from deeper sources. The heavier carbon isotopic signature of methane at the bottom of GC 51_{shelf} (Figure 5) suggests methane input from thermogenic sources [*Sauer et al*., 2015].

Table 6. Depth-Integrated Rates of AOM, POCSR, and ME in Units of µmol DIC cm^{-2} a^{-1}

	SMT Depth (m)	AOM	POCSR	ME	Total SR[a] (Fraction of Sulfate Reduction Coupled to AOM)
GC 36_{fjord}	1.62	18.8	57.4	3.6	47.5 (39.6%)
GC 51_{shelf}	1.10	56.4	3.4	2.4	58.1 (97.1%)

[a]Total SR = AOM + 0.5 POCSR (µmol sulfate cm^{-2} a^{-1}).

Our model estimates a 3 times higher AOM rate at GC 51_{shelf} compared to the rate at GC 36_{fjord} (Table 6). The AOM rate in Hola is higher but of the same order of magnitude as the rates estimated from a deep water site (~1200 m) west of Svalbard (up to 40.9 µmol DIC cm^{-2} a^{-1}) which is also an active methane seep site [*Hong et al*., 2016]. The rapid methane consumption rates suggest that AOM can

effectively prevent methane from leaking to the overlying bottom seawater in the fjord and at site GC 51_{shelf} on the shelf. However, recent studies in the Hola trough also reveal active seeps where gas is released to the water column due to methane-rich fluid ascent along certain pathways [*Chand et al*., 2008; *Sauer et al*., 2015] indicating that at these sites AOM capacity is not sufficient to consume all methane rising from below.

Generally, DIC in pore water is a mixture of different DIC sources, which have distinctly different $\delta^{13}C$ values. Buried seawater DIC has a $\delta^{13}C$ of around 0‰ [*Walter et al*., 2007], metabolic DIC is generated from mineralizing marine organic matter which has a $\delta^{13}C$ of −25‰ in GC 51_{shelf} and −21‰ in GC 36_{fjord}, and AOM can produce the lowest $\delta^{13}C$-DIC values depending on the $\delta^{13}C$ of the utilized methane. At GC 36_{fjord}, the overall organic matter decomposition rate is 61 μmol cm^{-2} a^{-1} (sum of POCSR and ME rates in Table 6) while at GC 51_{shelf} the rate of 5.8 μmol cm^{-2} a^{-1} is an order of magnitude lower. POSCR is responsible for 96% of the overall organic matter degradation at GC 36_{fjord} while only 67% of organic matter is degraded through POCSR at GC 51_{shelf}. As POCSR only causes negligible isotopic fractionation on carbon, the DIC produced by POCSR is assumed to have the same carbon isotopic signature as the organic matter [*Presley and Kaplan*, 1968]. Methanogenesis, on the other hand, has a large isotopic fractionation effect on carbon [*Whiticar*, 1999], resulting in a ^{13}C enrichment of DIC. At GC 36_{fjord}, POCSR dominates DIC production and therefore results in the carbon isotopic signature similar to the signature of organic matter (−21‰) at and above the SMT (Figure 5). The increase in $\delta^{13}C$-DIC toward the seafloor probably reflects the influence of seawater DIC. At both sites, the lowest $\delta^{13}C$-DIC values are found around the SMT which reflects the contribution of isotopically light DIC from AOM. The influence of ME on the $\delta^{13}C$-DIC below the SMT at both sites is indicated by the increase in $\delta^{13}C$-DIC with depth. This can be explained by the aging of pore water with depth and the continuous ^{13}C enrichment caused by ME. However, although ME rates at GC 36_{fjord} are higher, the shift to positive $\delta^{13}C$-DIC values at site GC 51_{shelf} is stronger (Figure 5) with values up to +18‰, whereas the highest value at GC 36_{fjord} is only −1.2‰. One explanation for the unexpected strong shift in $\delta^{13}C$-DIC at GC 51_{shelf} could be a smaller DIC pool due to low rates of POCSR and the potential removal of DIC by authigenic carbonate precipitation [*Sauer et al*., 2015]. A smaller DIC pool at GC 51_{shelf} compared to GC 36_{fjord} would mean that the relative contribution of ME to the DIC pool is larger and might explain the stronger shift to positive $\delta^{13}C$-DIC values at site GC 51_{shelf}. The lack of DIC concentration measurements, however, hampers the assessment of this hypothesis. An alternative explanation for isotopically heavier DIC in GC 51_{shelf} than in GC 36_{fjord} is the contribution of DIC from the deep-sourced fluid in the Hola trough. *Sauer et al*. [2015] reported signs of biodegradation of propane and *n*-butane in GC 51_{shelf} based on their $\delta^{13}C$ values. Several studies have shown a relationship between anaerobic hydrocarbon degradation and heavy $\delta^{13}C$ values of DIC or CO_2 [*Pallaser*, 2000; *Jones et al*., 2008; *Etiope et al*., 2009; *Milkov*, 2011]. This relationship is explained, first, by the formation of CO_2 due to the degradation of the higher molecular weight hydrocarbons and, secondly, by the subsequent secondary methanogenesis using the previously produced CO_2 which enriches the remaining CO_2 pool in ^{13}C [*Jones et al*., 2008]. This can lead to $\delta^{13}C$ values of CO_2 as positive as +27‰, as reported in a biodegraded petroleum accumulation in the West Siberian Basin [*Milkov*, 2010]. Thus, the ^{13}C-enriched DIC at depth in core GC 51_{shelf} could also be related to the contribution of isotopically heavy DIC from deeper fluids.

5.4. Gas Sources in Ullsfjorden and the Hola Trough

This section highlights the differences in gas sources between Ullsfjorden and the Hola trough (Figures 10 and 11). Our interpretation of gas sources is based on the $\delta^{13}C$ and $\delta^{2}H$ of methane, the $\delta^{13}C$ of DIC and also the $\delta^{13}C$ of ethane and propane [*Whiticar et al*., 1986; *Chung et al*., 1988; *Whiticar*, 1999; *Katz et al*., 2002; *Hinrichs et al*., 2006; *Vandré et al*., 2007]. Hydrocarbons in the Hola trough are thermogenic with only a minor contribution of microbial methane [*Sauer et al*., 2015]. This microbial methane can originate either from in situ methanogenesis, as shown by our pore water modeling, or secondary methanogenesis resulting from higher hydrocarbon degradation. In Ullsfjorden, we suggest a purely microbial source of methane. Even the higher hydrocarbons are probably formed by microbial processes as indicated by their low $\delta^{13}C$ values.

The predominance of thermogenic gaseous hydrocarbons from deeper sources in the Hola trough [*Sauer et al*., 2015] is inferred from significantly higher $\delta^{13}C$ values of methane, ethane and propane in GC 51_{shelf} compared to GC 36_{fjord} (Figure 11). A minor contribution of microbial methane is however suggested by $\delta^{13}C$ and $\delta^{2}H$ data of methane from core GC 51_{shelf} (Figure 10) that fall close to the range of methane

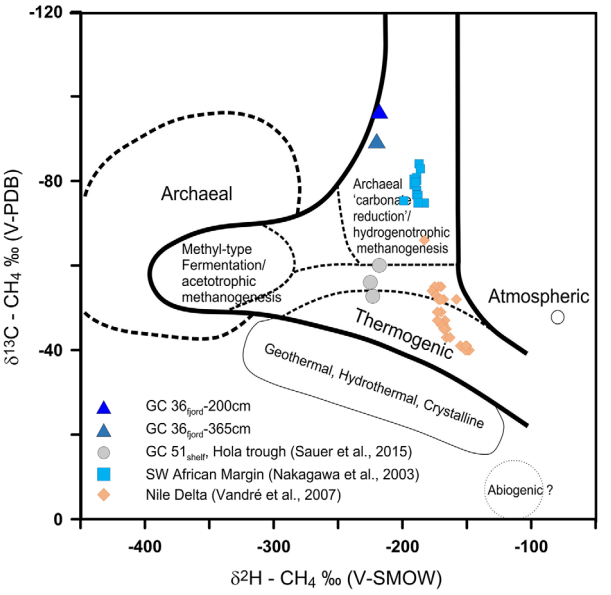

Figure 10. Plot of $\delta^{13}C$ of methane against $\delta^{2}H$ of methane. The fields of different methane sources are based on *Whiticar* [1999]. Analyses of samples from GC 36_{fjord} (blue triangles) plot clearly in the field of hydrogenotrophic methanogenesis.

produced by archaeal carbonate reduction. An additional source of microbial methane derives from the alternative interpretation of the isotopically heavy DIC in core GC 51_{shelf} being caused by anaerobic hydrocarbon degradation. The formation of isotopically heavy DIC in the deep reservoir requires secondary methanogenesis [*Jones et al.*, 2008]. Thus, the proportion of microbial methane in GC 51_{shelf} could be attributed to either primary methane production from in situ methanogenesis and/or to secondary microbial methane production through degradation of higher hydrocarbons. The relationship of anaerobic hydrocarbon degradation and secondary methanogenesis that results in ^{13}C-enriched fluids has been discussed in several studies, which found evidence of this process recorded in high $\delta^{13}C$ values of carbonates or CO_2 gas [*Dimitrakopoulos and Muehlenbachs*, 1987; *Pallaser*, 2000; *Crémière et al.*, 2012; *Crémière et al.*, 2013].

In Ullsfjorden, the contribution of thermogenic gases was considered unlikely [*Plassen*

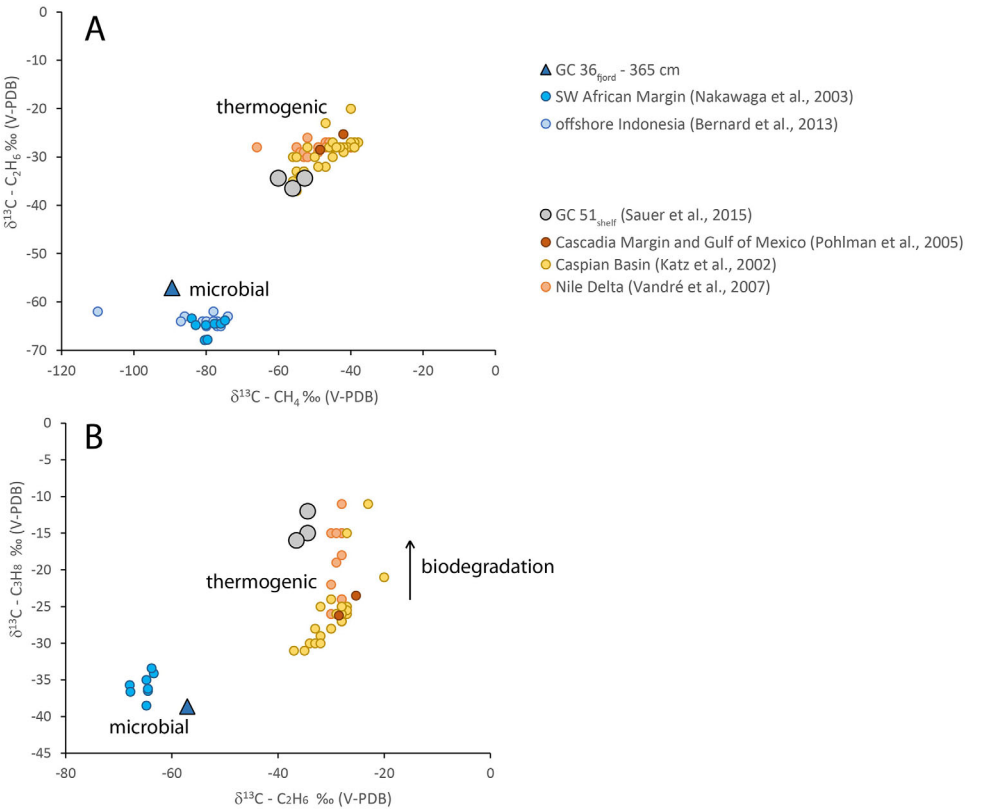

Figure 11. (a) Plot of $\delta^{13}C$-methane versus $\delta^{13}C$-ethane, and (b) plot of $\delta^{13}C$-ethane versus $\delta^{13}C$-propane. In both plots, we compare the gas isotope data from Ullsfjorden to data from the literature [*Katz et al.*, 2002; *Nakagawa et al.*, 2003; *Pohlman et al.*, 2005; *Vandré et al.*, 2007; *Bernard et al.*, 2013; *Sauer et al.*, 2015].

and Vorren, 2003a] which is strongly supported by our results. The methane $\delta^{13}C$ values of the Ullsfjorden samples are all below $-80‰$ and thus well within the range of microbial methane [*Whiticar*, 1999] (Figure 10). The two main pathways of microbial (archaeal) methanogenesis are via carbonate reduction, also called hydrogenotrophic methanogenesis or acetotrophic methanogenesis [*Botz et al*., 1996; *Conrad*, 2005; *Heuer et al*., 2009]. Carbon isotope fractionation is assumed to be stronger during hydrogenotrophic methanogenesis (fractionation factor up to 1.08) compared to acetotrophic methanogenesis (fractionation factor between 1.02 and 1.03) [*Whiticar*, 1999; *Conrad*, 2005]. Thus, the very low $\delta^{13}C$-CH_4 values of the Ullsfjorden gas samples down to $-96.5‰$ clearly favor hydrogenotrophic over acetotrophic methanogenesis in the fjord sediments (Figure 10). Depth profiles of $\delta^{13}C$ of methane and DIC in the methanogenic zone below the SMT in GC 36_{fjord} are likewise in accordance with hydrogenotrophic methanogenesis. $\delta^{13}C$-CH_4 and $\delta^{13}C$-DIC show the same gradients in this part of the core (200–380 cm, Figure 5), because of the constant fractionation factor between methane and DIC [*Whiticar*, 1999]. The parallel increase in both $\delta^{13}C$-CH_4 and $\delta^{13}C$-DIC with depth in GC 36_{fjord} is caused by a progressive enrichment of ^{13}C in the DIC pool, also causing progressive ^{13}C enrichment in the methane.

We detected ethane, propane, and butane in Ullsfjorden sediments, which are typically considered as indicators of thermogenic gas [e.g., *Bernard et al*., 1977; *Pohlman et al*., 2005]. The microbial origin of these higher hydrocarbons has, however, been proposed in earlier studies by incubation of sediment slurries [*Oremland et al*., 1988], for deep marine sediments from the south eastern Pacific [*Hinrichs et al*., 2006], for the Texas continental shelf and slope sediments [*Bernard et al*., 1978], and for shallow marine sediments offshore Indonesia [*Bernard et al*., 2013]. Based on our $\delta^{13}C$ values of ethane and propane (Figure 11), we suggest that also the higher molecular weight hydrocarbons in the Ullsfjorden sediments were formed by microbial processes. Figure 11 shows that the gases from Hola and Ullsfjorden are distinctly different in their isotopic composition. The samples from Hola have a similar composition to the gases from other localities with known thermogenic gas sources [*Katz et al*., 2002; *Pohlman et al*., 2005; *Vandré et al*., 2007] whereas the sample from Ullsfjorden is clearly dominated by gases with microbial origin [*Nakagawa et al*., 2003; *Bernard et al*., 2013]. The ethane $\delta^{13}C$ values of Ullsfjorden gas are much lower than is known and accepted for natural thermogenic gas [*Bernard et al*., 2013]. In the compilation of thermogenic gas by *Milkov* [2011], the $\delta^{13}C$ values of ethane range between $-40‰$ and $-14‰$, while ethane from Ullsfjorden has a $\delta^{13}C$ value of $-57‰$. Ethane with a light isotopic composition has also been reported by *Bernard et al*. [2013] and *Nakagawa et al*. [2003]. Their samples from shallow sediments offshore Indonesia and the SW African margin, respectively, exhibit $\delta^{13}C$-C_2 values between $-68‰$ and $-54‰$ and they propose a purely microbial origin to the gas. Moreover, the $\delta^{13}C$ values of propane from the Ullsfjorden gas samples are $-37.3‰$ and $-38.6‰$. These values are also lower than the range of thermogenic gas samples plotted in Figure 11b. We found no isotopic values of potential microbial butane in the literature yet. However, we assume that also the butane in the Ullsfjorden sediments is of microbial origin, because we are not aware of any mechanism that could result in a gas mixture of microbial methane, ethane and propane, and thermogenic butane.

6. Implications and Conclusion

Burial of organic carbon in marine sediments is an important part of the carbon cycle, especially in shelf and fjord settings, where significant amounts of organic carbon are sequestrated. In this study, we investigated two gravity cores from northern Norway, GC 51_{shelf} from the Hola trough on the continental shelf offshore the Vesterålen Islands and GC 36_{fjord} from Ullsfjorden, to understand the dynamics of supply and burial of organic matter in these settings (Table 7).

In the Hola trough, geochemical properties of organic matter ($\delta^{13}C$-C_{org} and C/N ratios) suggest the dominance of terrestrial organic matter delivery to the shelf. C_{org} accumulation in the Hola trough has been decreasing continuously since the last deglaciation as a result of both low organic matter supplies and erosional ocean bottom currents which prevent the deposition of the fine-grained-sediment-associated organic matter. Therefore, the continental shelf offshore the Vesterålen Islands, and potentially the majority of the Norwegian shelf north of the Lofoten Islands, play only a minor role in C_{org} sequestration as all these areas are presently characterized by an erosional sedimentary regime [*Bellec et al*., 2012]. However, during deglaciation the situation was different. Based on our study of GC 51_{shelf}, the sedimentation rates, fine-grained fraction and organic matter content were higher during deglaciation causing higher rates of C_{org} accumulation than at present.

Table 7. Summary of the Main Sedimentological and Organic Geochemical Characteristics of Core GC 36_{fjord} and GC 51_{shelf}

		GC 36_{FJORD}	GC 51_{SHELF}
SEDIMENTARY REGIME AND C_{ORG} BURIAL	Average SR	**High (73–129 cm ka^{-1})**	Low (9–80 cm ka^{-1})
	Grain size	Silt	Silt to sand
	C_{org} content	**High (2–3 wt %)**	Low (0.2–1.9 wt %)
	OM source	Dominantly marine	Dominantly terrestrial
	C_{org} AR Holocene	**1.2 g C cm^{-2} ka^{-1}**	Low (currently erosional)
EARLY DIAGENETIC REGIME AND GAS SOURCE	Organic matter degradation by POCSR and ME	**high**	low
	SMT	125–162 cm	**80–110 cm**
	Sulfate reduction	**60% POCSR**	3% POCSR
		40% AOM	**97% AOM**
	Carbon source for diagentic reactions	Marine C_{org} sedimentation (from above)	Methane seepage (from below)
	Gas source	Microbial	Thermogenic (+ primary and/or secondary microbial methane)

In Ullsfjorden, the high organic matter content and fast burial were sustained by the constant supply of marine organic matter from primary production over the last 4 ka. In light of previous studies of C_{org} sedimentation and burial, GC 36_{fjord} confirms the high rates of C_{org} burial in fjords supporting the view that fjords are hot spots of C_{org} accumulation [*Keil*, 2015; *Smith et al*., 2015]. This is supported by a compilation of CO_2 air-sea gas exchange measurements by *Chen et al*. [2013], stating that the majority of fjords are a sink of atmospheric CO_2.

The difference in sedimentation dynamics and C_{org} accumulation between the fjord and shelf setting strongly influences the early diagenetic processes in the sediments. As our model assessment on pore water profiles suggests, an order of magnitude more organic matter is degraded through sulfate reduction in the fjord than in the Hola trough. This is not surprising given the abundant labile marine organic matter supplied to the fjord sediment. Nonetheless, the SMT in the Hola trough is shallower than at the fjord site suggesting a faster sulfate turnover through AOM. Our model estimates that only a small fraction of AOM in the Hola trough is sustained by methane produced from in situ methanogenesis. Instead, the majority of AOM at this location is fueled by methane from a deeper thermogenic source [*Sauer et al*., 2015]. The methane in Ullsfjorden is proposed to originate exclusively from microbial processes sustained by the high input of C_{org} from settling MOM. Even the ethane and propane detected in our samples can be of microbial origin as suggested by their stable carbon isotopic signatures.

The investigation of gas composition and early diagenetic processes highlights the different carbon sources in the two settings. In Ullsfjorden, the carbon utilized by microbes for biogeochemical reaction is provided by settling organic matter from above, whereas on the Vesterålen shelf most of the carbon is provided by ascending methane from below.

Acknowledgments
We thank the captain and the crew of RV Helmer Hanssen for their support during the cruise. We are also grateful to Clea Fabian and Johan Faust for support during sampling at sea. We would further like to thank the NGU laboratory (Trondheim), the Inorganic Geochemistry lab at the Center for Marine Environmental Sciences, MARUM (Bremen), Stefano Bernasconi (ETH Zürich), and Serge Robert (EAWAG) for support during geochemical analyses. The data used are available in the tables, figures, supporting information, and cited references. Any additional data may be obtained from the corresponding author (simone11sauer@gmail.com). We thank Susann Henkel and an anonymous reviewer for their very helpful and constructive comments on earlier versions of the manuscript. The authors acknowledge funding from RWE-DEA (now DEA; C-1648/1) and from the Norwegian Research Council through its Centres of Excellence funding scheme (project number 223259) for CAGE—Centre for Arctic Gas Hydrate, Environment and Climate, Department of Geology, UiT, The Arctic University of Norway, Tromsø, Norway and Petromaks2 NORCRUST - Norwegian margin fluid systems and methane-derived authigenic carbonate crusts (project number 255150).

References

Bauer, J. E., W.-J. Cai, P. A. Raymond, T. S. Bianchi, C. S. Hopkinson, and P. A. G. Regnier (2013), The changing carbon cycle of the coastal ocean, *Nature*, *504*(7478), 61–70.

Bellec, V., R. Bøe, T. Thorsnes, L. Rise, M. Dolan, S. Elvenes, A. Lepland, and O. H. Selboskar (2012), Geologisk Havbunnskart, Kart 6183001400, Norg. Geol. Undersøkelse, Trondheim.

Bernard, B., J. M. Brooks, and W. M. Sackett (1977), A geochemical model for characterization of hydrocarbon gas sources in marine sediments, in *Proceedings of 9th Offshore Technology Conference*, Houston, Tex.

Bernard, B. B., J. M. Brooks, and W. M. Sackett (1978), Light hydrocarbons in recent Texas continental shelf and slope sediments, *J. Geophys. Res.*, *83*(C8), 4053–4061.

Bernard, B. B., D. L. Orange, J. M. Brooks, and J. Decker (2013), Interstitial light hydrocarbon gases in jumbo piston cores offshore Indonesia: Thermogenic or biogenic?, in *Proceedings of 9th Offshore Technology Conference*, American Association of Petroleum Geologists (AAPG), American Institute of Chemical Engineers (AIChE), American Institute of Mining, Metallurgical, and Petroleum Engineers (AIME), American Society of Civil Engineers (ASCE), American Society of Mechanical Engineers (ASME), Institute of Electrical and Electronics Engineers, Oceanic and Engineering Society (IEEE-OES), Marine Technology Society (MTS), Society of Exploration Geophysicists (SEG), Society for Mining, Metallurgy, and Exploration Inc. (SME), Society of Naval Architects and Marine Engineers (SNAME), Society of Petroleum Engineers (SPE) , The Minerals, Metals, and Materials Society (TMS), Brazilian Petroleum, Gas and Biofuels Institute (IBP), Houston, Tex.

Berner, R. A. (1980), *Early Diagenesis: A Theoretical Approach*, Princeton Univ. Press, Princeton, N. J.

Berner, R. A. (1982), Burial of organic carbon and pyrite sulfur in the modern ocean: Its geochemical and environmental significance, *Am. J. Sci.*, *282*(4), 451–473.

Bhatnagar, G., W. G. Chapman, G. R. Dickens, B. Dugan, and G. J. Hirasaki (2008), Sulfate-methane transition as a proxy for average methane hydrate saturation in marine sediments, *Geophys. Res. Lett.*, *35*, L03611, doi:10.1029/2007GL032500.

Bianchi, T. S., and J. E. Bauer (2011), Particulate organic carbon cycling and transformation, in *Treatise on Estuarine and Coastal Science*, edited by E. Wolanski and D. McLusky, chap. 5.03, pp. 69–117, Academic, Waltham, Mass.
Blaauw, M. (2010), Methods and code for 'classical' age-modelling of radiocarbon sequences, *Quat. Geochronol.*, *5*(5), 512–518.
Bøe, R., V. K. Bellec, M. F. J. Dolan, P. Buhl-Mortensen, L. Buhl-Mortensen, D. Slagstad, and L. Rise (2009), Giant sandwaves in the Hola glacial trough off Vesterålen, North Norway, *Mar. Geol.*, *267*(1–2), 36–54.
Bøe, R., et al. (2015), Sandwaves and sand transport on the Barents Sea continental slope offshore northern Norway, *Mar. Pet. Geol.*, *60*, 34–53.
Boetius, A., and F. Wenzhöfer (2013), Seafloor oxygen consumption fuelled by methane from cold seeps, *Nat. Geosci.*, *6*(9), 725–734.
Boetius, A., K. Ravenschlag, C. J. Schubert, D. Rickert, F. Widdel, A. Gieseke, R. Amann, B. B. Jorgensen, U. Witte, and O. Pfannkuche (2000), A marine microbial consortium apparently mediating anaerobic oxidation of methane, *Nature*, *407*(6804), 623–626.
Borowski, W. S., C. K. Paull, and W. Ussler (1996), Marine pore-water sulfate profiles indicate in situ methane flux from underlying gas hydrate, *Geology*, *24*(7), 655–658.
Borowski, W. S., C. K. Paull, and W. Ussler Iii (1999), Global and local variations of interstitial sulfate gradients in deep-water, continental margin sediments: Sensitivity to underlying methane and gas hydrates, *Mar. Geol.*, *159*(1–4), 131–154.
Botz, R., H.-D. Pokojski, M. Schmitt, and M. Thomm (1996), Carbon isotope fractionation during bacterial methanogenesis by CO_2 reduction, *Org. Geochem.*, *25*(3–4), 255–262.
Bowles, M. W., J. M. Mogollon, S. Kasten, M. Zabel, and K. U. Hinrichs (2014), Global rates of marine sulfate reduction and implications for sub-sea-floor metabolic activities, *Science*, *344*(6186), 889–891.
Cai, W.-J., M. Dai, and Y. Wang (2006), Air-sea exchange of carbon dioxide in ocean margins: A province-based synthesis, *Geophys. Res. Lett.*, *33*, L12603, doi:10.1029/2006GL026219.
Chand, S., L. Rise, V. Bellec, M. Dolan, R. Bøe, T. Thorsnes, and P. Buhl-Mortensen (2008), Active venting system offshore Northern Norway, *Eos Trans. AGU*, *89*(29), 261–262.
Chen, C. T. A., T. H. Huang, Y. C. Chen, Y. Bai, X. He, and Y. Kang (2013), Air–sea exchanges of CO_2 in the world's coastal seas, *Biogeosciences*, *10*(10), 6509–6544.
Chung, H. M., J. R. Gormly, and R. M. Squires (1988), Origin of gaseous hydrocarbons in subsurface environments: Theoretical considerations of carbon isotope distribution, *Chem. Geol.*, *71*(1–3), 97–104.
Conrad, R. (2005), Quantification of methanogenic pathways using stable carbon isotopic signatures: A review and a proposal, *Org. Geochem.*, *36*(5), 739–752.
Crémière, A., C. Pierre, M.-M. Blanc-Valleron, T. Zitter, M. N. Çağatay, and P. Henry (2012), Methane-derived authigenic carbonates along the North Anatolian fault system in the Sea of Marmara (Turkey), *Deep Sea Res., Part I*, *66*, 114–130.
Crémière, A., G. Bayon, E. Ponzevera, and C. Pierre (2013), Paleo-environmental controls on cold seep carbonate authigenesis in the Sea of Marmara, *Earth Planet. Sci. Lett.*, *376*, 200–211.
Dearing, J. A. (1994), *Environmental Magnetic Susceptibility: Using the Bartington MS2 System*, Chi Publ., Kenilworth, UK.
de Haas, H., T. C. E. van Weering, and H. de Stigter (2002), Organic carbon in shelf seas: Sinks or sources, processes and products, *Cont. Shelf Res.*, *22*(5), 691–717.
Dickens, G. R., D. Schroeder, K.-U. Hinrichs, and Leg 201 Scientific Party (2003), The pressure core sampler (PCS) on ODP Leg 201: General operations and gas release, in *Proceedings of the Ocean Drilling Program, Initial Reports*, vol. 201, edited by S. L. D'Hondt et al., pp. 1–22, U.S. Gov. Print. Off., Washington, D. C.
Dimitrakopoulos, R., and K. Muehlenbachs (1987), Isotopes in the sedimentary cycle biodegradation of petroleum as a source of ^{13}C-enriched carbon dioxide in the formation of carbonate cement, *Chem. Geol.*, *65*(3), 283–291.
Elvsborg, A. (1979), Late Quaternary sedimentation in a glacial trough on the continental shelf off Troms, northern Norway, *Norsk Geol. Tidsskrift*, *59*, 309–325.
Etiope, G., A. Feyzullayev, A. V. Milkov, A. Waseda, K. Mizobe, and C. H. Sun (2009), Evidence of subsurface anaerobic biodegradation of hydrocarbons and potential secondary methanogenesis in terrestrial mud volcanoes, *Mar. Pet. Geol.*, *26*(9), 1692–1703.
Farquhar, G. D., J. R. Ehleringer, and K. T. Hubick (1989), Carbon isotope discrimination and photosynthesis, *Annu. Rev. Plant Physiol. Plant Mol. Biol.*, *40*(1), 503–537.
Fenchel, T., G. M. King, and T. H. Blackburn (1998), *Bacterial Biogeochemistry: The Ecophysiology of Mineral Cycling*, Academic, San Diego, Calif.
Fenchel, T., G. M. King, and T. H. Blackburn (2012a), Degradation of organic polymers and hydrocarbons, in *Bacterial Biogeochemistry*, 3rd ed., edited by T. Blackburn, T. Fenchel, and G. M. King, chap. 3, pp. 49–57, Academic, Boston, Mass.
Fenchel, T., G. M. King, and T. H. Blackburn (2012b), The water column, in *Bacterial Biogeochemistry*, 3rd ed., edited by T. Blackburn, G. M. Fenchel, and T. H. King, chap. 5, pp. 67–88, Academic, Boston, Mass.
Forwick, M., and T. O. Vorren (2009), Late Weichselian and holocene sedimentary environments and ice rafting in Isfjorden, Spitsbergen, *Palaeogeogr. Palaeoclimatol. Palaeoecol.*, *280*(1–2), 258–274.
Haeckel, M., I. König, V. Riech, M. E. Weber, and E. Suess (2001), Pore water profiles and numerical modelling of biogeochemical processes in Peru Basin deep-sea sediments, *Deep Sea Res., Part II*, *48*(17–18), 3713–3736.
Hall, I. R., and I. N. McCave (1998), Glacial-interglacial variation in organic carbon burial on the slope of the N.W. European Continental Margin (48°–50°N), *Prog. Oceanogr.*, *42*(1–4), 37–60.
Hall, P. O. J., and R. C. Aller (1992), Rapid, small-volume, flow injection analysis for CO_2, and NH^{4+} in marine and freshwaters, *Limnol. Oceanogr.*, *35*, 1113–1119.
Hansen, J. W., S. Bakke, and S. Fanavoll (1992), Shallow drilling Nordland VI and VII 1991, *IKU Rep. 23*, IKU, Sintef Group, Trondheim.
Hartnett, H. E., R. G. Keil, J. I. Hedges, and A. H. Devol (1998), Influence of oxygen exposure time on organic carbon preservation in continental margin sediments, *Nature*, *391*(6667), 572–575.
Hedges, J. I., and R. G. Keil (1995), Sedimentary organic matter preservation: An assessment and speculative synthesis, *Mar. Chem.*, *49*(2–3), 81–115.
Henrichs, S. M. (1992), Early diagenesis of organic matter in marine sediments: Progress and perplexity, *Mar. Chem.*, *39*(1–3), 119–149.
Heuer, V. B., J. W. Pohlman, M. E. Torres, M. Elvert, and K.-U. Hinrichs (2009), The stable carbon isotope biogeochemistry of acetate and other dissolved carbon species in deep subseafloor sediments at the northern Cascadia Margin, *Geochim. Cosmochim. Acta*, *73*(11), 3323–3336.
Hinrichs, K.-U., J. M. Hayes, S. P. Sylva, P. G. Brewer, and E. F. DeLong (1999), Methane-consuming archaebacteria in marine sediments, *Nature*, *398*(6730), 802–805.
Hinrichs, K.-U., J. M. Hayes, W. Bach, A. J. Spivack, L. R. Hmelo, N. G. Holm, C. G. Johnson, and S. P. Sylva (2006), Biological formation of ethane and propane in the deep marine subsurface, Proc. *Natl. Acad. Sci. U. S. A.*, *103*(40), 14,684–14,689.
Hong, W.-L., E. A. Solomon, and M. E. Torres (2014a), A kinetic-model approach to quantify the effect of mass transport deposits on pore water profiles in the Krishna–Godavari Basin, *Bay of Bengal, Mar. Pet. Geol.*, *58*, 223–232.

Hong, W.-L., M. E. Torres, J.-H. Kim, J. Choi, and J.-J. Bahk (2014b), Towards quantifying the reaction network around the sulfate–methane-transition-zone in the Ulleung Basin, East Sea, with a kinetic modeling approach, *Geochim. Cosmochim. Acta*, *140*, 127–141.
Hong, W.-L., S. Sauer, G. Panieri, W. G. Ambrose, R. H. James, A. Plaza-Faverola, and A. Schneider (2016), Removal of methane through hydrological, microbial, and geochemical processes in the shallow sediments of pockmarks along eastern Vestnesa Ridge (Svalbard), *Limnol. Oceanogr.*, doi:10.1002/lno.10299, in press.
Hounslow, M. W., and B. A. Maher (1999), Source of the climate signal recorded by magnetic susceptibility variations in Indian Ocean sediments, *J. Geophys. Res.*, *104*(B3), 5047–5061.
Hovland, M., and A. G. Judd (1988), *Seabed Pockmarks and Seepages. Impact on Geology, Biology and Marine Environment*, 293 pp., Graham and Trotman, London.
Johnson, M. A., N. H. Kenyon, R. H. Belderson, and A. H. Stride (1982), *Sand transport, in Offshore Tidal Sands*, edited by A. H. Stride, pp. 58–94, Springer, Dordrecht, Netherlands.
Jones, D. M., et al. (2008), Crude-oil biodegradation via methanogenesis in subsurface petroleum reservoirs, *Nature*, *451*(7175), 176–180.
Kasten, S., M. Zabel, V. Heuer, and C. Hensen (2004), Processes and signals of nonsteady-state diagenesis in deep-sea sediments and their pore waters, in *The South Atlantic in the Late Quaternary: Reconstruction of Material Budgets and Current Systems*, edited by G. Wefer, S. Mulitza, and V. Ratmeyer, pp. 431–459, Springer, Berlin.
Katz, B. J., A. Narimanov, and R. Huseinzadeh (2002), Significance of microbial processes in gases of the South Caspian basin, *Mar. Pet. Geol.*, *19*(6), 783–796.
Keil, R. (2015), Carbon cycle: Hoard of fjord carbon, *Nat. Geosci.*, *8*(6), 426–427.
Knies, J., and P. Martinez (2009), Organic matter sedimentation in the western Barents Sea region: Terrestrial and marine contribution based on isotopic composition and organic nitrogen content, *Norw. J. Geol.*, *89*(1/2), 79–89.
Knies, J., M. Hald, H. Ebbesen, U. Mann, and C. Vogt (2003), A deglacial–middle Holocene record of biogenic sedimentation and paleoproductivity changes from the northern Norwegian continental shelf, *Paleoceanography*, *18*(4), 1096, doi:10.1029/2002PA000872.
Krom, M. D., and R. A. Berner (1980), Adsorption of phosphate in anoxic marine sediments, *Limnol. Oceanogr.*, *25*(5), 797–806.
Laberg, J. S., et al. (2005), Cenozoic alongslope processes and sedimentation on the NW European Atlantic margin, *Mar. Pet. Geol.*, *22*(9–10), 1069–1088.
Langrock, U. (2004), *Late Jurassic to Early Cretaceous Black Shale Formation and Paleoenvironment in High Northern Latitudes*, Univ. of Bremen, Bremen, Germany.
Laruelle, G. G., H. H. Dürr, C. P. Slomp, and A. V. Borges (2010), Evaluation of sinks and sources of CO_2 in the global coastal ocean using a spatially-explicit typology of estuaries and continental shelves, *Geophys. Res. Lett.*, *37*, L15607, doi:10.1029/2010GL043691.
Lehmann, M. F., S. M. Bernasconi, A. Barbieri, and J. A. McKenzie (2002), Preservation of organic matter and alteration of its carbon and nitrogen isotope composition during simulated and in situ early sedimentary diagenesis, *Geochim. Cosmochim. Acta*, *66*(20), 3573–3584.
Li, Y.-H., and S. Gregory (1974), Diffusion of ions in sea water and in deep-sea sediments, Geochim. *Cosmochim. Acta*, *38*(5), 703–714.
Meister, P., B. Liu, T. G. Ferdelman, B. B. Jørgensen, and A. Khalili (2013), Control of sulphate and methane distributions in marine sediments by organic matter reactivity, *Geochim. Cosmochim. Acta*, *104*, 183–193.
Meyers, P. A. (1994), Preservation of elemental and isotopic source identification of sedimentary organic matter, *Chem. Geol.*, *114*(3), 289–302.
Milkov, A. V. (2010), Methanogenic biodegradation of petroleum in the West Siberian Basin (Russia): Significance for formation of giant Cenomanian gas pools, *AAPG Bull.*, *94*(10), 1485–1541.
Milkov, A. V. (2011), Worldwide distribution and significance of secondary microbial methane formed during petroleum biodegradation in conventional reservoirs, *Org. Geochem.*, *42*(2), 184–207.
Müller, P. J., and E. Suess (1979), Productivity, sedimentation rate, and sedimentary organic matter in the oceans—I. Organic carbon preservation, *Deep Sea Res., Part A*, *26*(12), 1347–1362.
Murphy, J., and J. P. Riley (1962), A modified single solution method for the determination of phosphate in natural waters, *Anal. Chim. Acta*, *27*, 31–36.
Nakagawa, F., U. Tsunogai, N. Yoshida, and D. D. Adams (2003), Stable isotopic compositions of bacterial light hydrocarbons in marginal marine sediments, in *Land and Marine Hydrogeology*, edited by M. T. W. G. Taniguchi, K. Wang, and T. Gamo, chap. 8, pp. 141–150, Elsevier, Amsterdam.
Nauhaus, K., A. Boetius, M. Krüger, and F. Widdel (2002), In vitro demonstration of anaerobic oxidation of methane coupled to sulphate reduction in sediment from a marine gas hydrate area, *Environ. Microbiol.*, *4*(5), 296–305.
Nowaczyk, N. R. (2002), Logging of magnetic susceptibility, in *Tracking Environmental Change Using Lake Sediments*, edited by W. M. Last, and J. P. Smol, pp. 155–170, Kluwer Acad., Dordrecht, Netherlands.
Oremland, R. S., M. J. Whiticar, F. E. Strohmaier, and R. P. Kiene (1988), Bacterial ethane formation from reduced, ethylated sulfur compounds in anoxic sediments, *Geochim. Cosmochim. Acta*, *52*(7), 1895–1904.
Orphan, V. J., C. H. House, K.-U. Hinrichs, K. D. McKeegan, and E. F. DeLong (2001), Methane-consuming archaea revealed by directly coupled isotopic and phylogenetic analysis, *Science*, *293*(5529), 484–487.
Pallaser, R. J. (2000), Recognising biodegradation in gas/oil accumulations through the [dgr]13C composition of gas components, *Org. Geochem.*, *31*, 1363-1373.
Plassen, L., and T. O. Vorren (2003a), Fluid flow features in fjord-fill deposits, Ullsfjorden, North Norway, Norw. *J. Geol.*, *83*, 37–42.
Plassen, L., and T. O. Vorren (2003b), Sedimentary processes and the environment during deglaciation of a fjord basin in Ullsfjorden, North Norway, Norw. *J. Geol.*, *83*, 23–26.
Pohlman, J. W., E. A. Canuel, N. R. Chapman, G. D. Spence, M. J. Whiticar, and R. B. Coffin (2005), The origin of thermogenic gas hydrates on the northern Cascadia Margin as inferred from isotopic ($^{13}C/^{12}C$ and D/H) and molecular composition of hydrate and vent gas, *Org. Geochem.*, *36*(5), 703–716.
Pohlman, J. W., M. Riedel, J. E. Bauer, E. A. Canuel, C. K. Paull, L. Lapham, K. S. Grabowski, R. B. Coffin, and G. D. Spence (2013), Anaerobic methane oxidation in low-organic content methane seep sediments, *Geochim. Cosmochim. Acta*, *108*, 184–201.
Presley, B. J., and I. R. Kaplan (1968), Changes in dissolved sulfate, calcium and carbonate from interstitial water of near-shore sediments, *Geochim. Cosmochim. Acta*, *32*(10), 1037–1048.
Rau, G. H., R. E. Sweeney, and I. R. Kaplan (1982), Plankton ^{13}C: ^{12}C ratio changes with latitude: Differences between northern and southern oceans, *Deep Sea Res., Part A*, *29*(8), 1035–1039.
Reeburgh, W. S. (2007), Oceanic methane biogeochemistry, *Chem. Rev.*, *107*(2), 486–513.
Reimer, P. J., et al. (2013), IntCal13 and marine13 radiocarbon age calibration curves 0–50,000 years cal BP, *Radiocarbon*, *55*(4), 1869–1887.

Riedinger, N., K. Pfeifer, S. Kasten, J. F. L. Garming, C. Vogt, and C. Hensen (2005), Diagenetic alteration of magnetic signals by anaerobic oxidation of methane related to a change in sedimentation rate, *Geochim. Cosmochim. Acta*, *69*(16), 4117–4126.
Sauer, S. (2016), *Past and Present Natural Methane Seepage on the Northern Norwegian Continental Shelf*, 194 pp., Arctic Univ., Tromsø, Norway.
Sauer, S., J. Knies, A. Lepland, S. Chand, F. Eichinger, and C. J. Schubert (2015), Hydrocarbon sources of cold seeps off the Vesterålen coast, northern Norway, *Chem. Geol.*, *417*, 371–382.
Schubert, C. J., and S. E. Calvert (2001), Nitrogen and carbon isotopic composition of marine and terrestrial organic matter in Arctic Ocean sediments: Implications for nutrient utilization and organic matter composition, *Deep Sea Res., Part I*, *48*(3), 789–810.
Seeberg-Elverfeldt, J., M. Schlüter, T. Feseker, and M. Kölling (2005), Rhizon sampling of porewaters near the sediment-water interface of aquatic systems, *Limnol. Oceanogr. Methods*, *3*(8), 361–371.
Smelror, M., A. Mørk, M. B. E. Mørk, H. M. Weiss, and H. Løseth (2001), Middle Jurassic-lower cretaceous transgressive-regressive sequences and facies distribution off northern Nordland and Troms, Norway, in *Sedimentary Environments Offshore Norway—Palaeozoic to Recent, Norw. Pet. Soc. Spec. Publ.*, edited by J. M. Ole and D. Tom, pp. 211–232, Elsevier, Amsterdam.
Smith, R. W., T. S. Bianchi, M. Allison, C. Savage, and V. Galy (2015), High rates of organic carbon burial in fjord sediments globally, *Nat. Geosci.*, *8*, 450–453.
Sommer, S., O. Pfannkuche, P. Linke, R. Luff, J. Greinert, M. Drews, S. Gubsch, M. Pieper, M. Poser, and T. Viergutz (2006), Efficiency of the benthic filter: Biological control of the emission of dissolved methane from sediments containing shallow gas hydrates at Hydrate Ridge, *Global Biogeochem. Cycles*, *20*, GB2019, doi:10.1029/2004GB002389.
Steefel, C. I. (2009), CrunchFlow—Software for Modeling Multicomponent Reactive Flow and Transport, Lawrence Berkeley National Laboratory, Berkeley, Calif.
Steefel, C. I., J. L. Druhan, and K. Maher (2014), Modeling coupled chemical and isotopic equilibration rates, *Proc. Earth Planet. Sci.*, *10*, 208–217.
Steefel, C.I., et al. (2015), Reactive transport codes for subsurface environmental simulation, *Comput. Geosci.*, *19*(3), 445–478.
St-Onge, G., and C. Hillaire-Marcel (2001), Isotopic constraints of sedimentary inputs and organic carbon burial rates in the Saguenay Fjord, Quebec. *Mar. Geol.*, *176*(1–4), 1-22.
Teeri, J. A., and L. G. Stowe (1976), Climatic patterns and the distribution of C4 grasses in North America, *Oecologia*, *23*(1), 1–12.
Tyson, R. V. (1995), *Sedimentary Organic Matter: Organic Facies and Palynofacies*, Chapman and Hall, London.
Vandré, C., B. Cramer, P. Gerling, and J. Winsemann (2007), Natural gas formation in the western Nile delta (Eastern Mediterranean): Thermogenic versus microbial, *Org. Geochem.*, *38*(4), 523–539.
Vavilin, V. (2013), Estimating changes of isotopic fractionation based on chemical kinetics and microbial dynamics during anaerobic methane oxidation: Apparent zero-and first-order kinetics at high and low initial methane concentrations, *Antonie van Leeuwenhoek*, *103*(2), 375–383.
Vorren, T. O., and L. I. V. Plassen (2002), Deglaciation and palaeoclimate of the Andfjord-Vågsfjord area, North Norway, *Boreas*, *31*(2), 97–125.
Vorren, T. O., M. Hald, and E. Thomsen (1984), Quaternary sediments and environments on the continental shelf off northern Norway, *Mar. Geol.*, *57*(1–4), 229–257.
Vorren, T. O., E. Lebesbye, K. Andreassen, and K. B. Larsen (1989), Glacigenic sediments on a passive continental margin as exemplified by the Barents Sea, *Mar. Geol.*, *85*(2–4), 251–272.
Vorren, T. O., T. A. Rydningen, N. J. Baeten, and J. S. Laberg (2015), Chronology and extent of the Lofoten–Vesterålen sector of the Scandinavian Ice Sheet from 26 to 16 cal. ka BP, *Boreas*, *44*, 445–458.
Wallmann, K., G. Aloisi, M. Haeckel, A. Obzhirov, G. Pavlova, and P. Tishchenko (2006), Kinetics of organic matter degradation, microbial methane generation, and gas hydrate formation in anoxic marine sediments, *Geochim. Cosmochim. Acta*, *70*(15), 3905–3927.
Walter, L. M., T. C. W. Ku, K. Muehlenbachs, W. P. Patterson, and L. Bonnell (2007), Controls on the δ13C of dissolved inorganic carbon in marine pore waters: An integrated case study of isotope exchange during syndepositional recrystallization of biogenic carbonate sediments (South Florida Platform, USA), *Deep Sea Res., Part II*, *54*(11-13), 1163–1200.
Weber, M. E., F. Niessen, G. Kuhn, and M. Wiedicke (1997), Calibration and application of marine sedimentary physical properties using a multi-sensor core logger, *Mar. Geol.*, *136*(3–4), 151–172.
Wegener, G., and A. Boetius (2009), An experimental study on short-term changes in the anaerobic oxidation of methane in response to varying methane and sulfate fluxes, *Biogeosciences*, *6*(5), 867–876.
Whiticar, M. J. (1999), Carbon and hydrogen isotope systematics of bacterial formation and oxidation of methane, *Chem. Geol.*, *161*(1–3), 291–314.
Whiticar, M. J., E. Faber, and M. Schoell (1986), Biogenic methane formation in marine and freshwater environments: CO_2 reduction vs. acetate fermentation—Isotope evidence, *Geochim. Cosmochim. Acta*, *50*(5), 693–709.
Winkelmann, D., and J. Knies (2005), Recent distribution and accumulation of organic carbon on the continental margin west off Spitsbergen, *Geochem. Geophys. Geosyst.*, *6*, Q09012, doi:10.1029/2005GC000916.
Wollast, R. (1991), The coastal organic carbon cycle: Fluxes, sources and sinks, in *Ocean Margin Processes in Global Change, Dahlem Workshop Reports*, edited by R. F. C. Mantoura, J.-M. Martin, and R. Wollast, pp. 365–381, Wiley-Intersci., Chichester, U. K.
Yoshinaga, M. Y., C. S. Lazar, M. Elvert, Y.-S. Lin, C. Zhu, V. B. Heuer, A. Teske, and K.-U. Hinrichs (2015), Possible roles of uncultured archaea in carbon cycling in methane-seep sediments, *Geochim. Cosmochim. Acta*, *164*, 35–52.
Yu, F., Y. Zong, J. M. Lloyd, G. Huang, M. J. Leng, C. Kendrick, A. L. Lamb, and W. W. S. Yim (2010), Bulk organic δ13C and C/N as indicators for sediment sources in the Pearl River delta and estuary, southern China, *Estuarine Coastal Shelf Sci.*, *87*(4), 618–630.
Zhang, S., L. Yang, D. J. DePaolo, and C. I. Steefel (2015), Chemical affinity and pH effects on chlorite dissolution kinetics under geological CO_2 sequestration-related conditions, Chem. *Geol.*, *396*, 208–217.